Journal of Hydrology 600 (2021) 126568

Contents lists available at ScienceDirect

Journal of Hydrology

journal homepage: www.elsevier.com/locate/jhydrol

Research papers

1D-4D electrical and electromagnetic methods revealing fault-controlled aquifer geometry and saline water uprising

Patrizio Torrese *, Giorgio Pilla

Università di Pavia, Dipartimento di Scienze della Terra e dell'Ambiente, Pavia, Italy

ARTICLE INFO

This manuscript was handled by C. Corradini, Editor-in-Chief, with the assistance of Stephen Worthington, Associate Editor

Keywords:
Electrical resistivity
Electromagnetics
Time-lapse
Hydrogeological model
Aquifer geometry
Saline paleo-water uprising
Vogherese fault
Hydro-geophysics

ABSTRACT

This paper presents new results of 1D-4D electrical resistivity and electromagnetic surveys for the delineation of aquifer geometry and the detection of saline paleo-water uprising along structural discontinuities. These geophysical surveys were undertaken at the alluvial aquifer of the Oltrepò Pavese plain sector (Po Valley, Northern Italy). At the investigated test site, the alluvial aquifer is strongly conditioned by the presence of an important tectonic discontinuity whose localization and trace were better defined by this study. This fault is responsible for the sudden deepening that affects the bedrock and is also responsible for the uprising of deep, saline paleo-waters which strongly influences the chemistry of groundwater.

During the campaign a variety of experimental setups were tested. This provided an ideal opportunity to cross-validate geophysical results with extensive ground truth provided by groundwater sampling and stratigraphic, electrical conductivity, temperature and redox potential logs undertaken within the wells. It also permitted an assessment of the usability of electrical and electromagnetic surveys in such a complex hydrogeological setting.

Geophysical surveys revealed the presence of sharp and irregular contact between the alluvial aquifer and the underlying bedrock. This is characterized by morphological irregularities, which are likely to have been shaped either by tectonics and/or by the paleo-river's erosion. The bedrock is affected by saline water contaminations which are likely localized along structural discontinuities which represent and facilitate the flow towards the alluvial aquifer. Detailed 3D and time-lapse imaging revealed irregular-shaped shallow saline water contaminations within the alluvial aquifer, as well as temporal variability of groundwater salinity. Spatial distribution of contaminations and salinity degree are likely to be affected by different factors like the aperture of the discontinuities within the bedrock, the hydraulic conductivity of the aquifer, as well as seasonal variations in terms of fresh water recharge.

1. Introduction

Among various geophysical methods potentially useful in solving a wide spectrum of prospecting and investigation problems when studying aquifers (e.g., seismic, micro-gravimetric and time-domain electromagnetic methods) electrical resistivity and electromagnetic methods are well-suited geophysical techniques to investigate and partially characterize shallow aquifers.

There have been many applications of Electrical Resistivity Tomography (ERT) and electrical methods in general to characterize aquifers (Coscia et al., 2011; Kazakis et al., 2016a, 2016b; Meyerhoff et al., 2014; Vogelgesang et al., 2020), delineate alluvial aquifer heterogeneity (Bowling et al., 2005), thickness and bedrock structure (Gómez et al., 2019), monitor hydraulic processes (Kuras et al., 2009) and aquifer discharge (Meyerhoff et al., 2012), map saline water contaminations (Kazakis et al., 2016a, 2016b; Rainone et al., 2015), as well as detect karst features (Torrese, 2020), sinkholes and cavities (Torrese et al., 2021; Van Schoor, 2002).

Very Low Frequency Electromagnetic (VLF-EM) has been typically used for the identification of fracture zones for groundwater exploration (Jamal and Singh, 2018), detection of fractures in the bedrock (Adepelumi et al., 2006), geological boundaries and shear zones/faults (Gnaneshwar et al., 2011), but it has been also applied to map groundwater condition in sedimentary basins (Ohwoghere-Asuma et al., 2020) and detect leachate plumes and groundwater pollution (Al-Tarazi et al., 2008).

This study involves electrical resistivity and VLF-EM methods due to their ability in detecting conductive bodies which represent the main

* Corresponding author.
E-mail address: patrizio.torrese@unipv.it (P. Torrese).

https://doi.org/10.1016/j.jhydrol.2021.126568
Received 9 February 2021; Received in revised form 3 June 2021; Accepted 9 June 2021
Available online 11 June 2021

geophysical targets of this research project. In the investigated hydrogeological setting, conductive bodies are related to saline water contaminations within the alluvial aquifer or along structural discontinuities within the bedrock, as well as they are related to the clayey hydrogeological bedrock. If the VLF-EM method provides quick detection of well-coupled conductive bodies, electrical resistivity methods provide more accurate and complete models. Furthermore, electrical resistivity methods allow to outline the vertical and horizontal distribution of both low (e.g., fine-grained alluvial layers) and high (e.g., coarse-grained alluvial layers) resistivity bodies.

Although 1D geophysical surveys allow to define subsoil layering and main geological boundaries, 2D and especially 3D surveys allow to obtain more accurate and complete geophysical models and better define aquifer heterogeneity; 4D surveys, usually termed time-lapse surveys, where the fourth dimension is time, allow to monitor time-varying processes, such as groundwater contamination.

The objectives of the study are to test the suitability of 1D-4D electrical resistivity and VLF-EM methods for the delineation of aquifer geometry and the detection of saline paleo-water uprising along structural discontinuities and to verify advantages and limitations of the methods in a complex hydrogeological setting. At the investigated test site, the hydrogeological clayey bedrock may be affected by morphological irregularities and saline water contaminations; furthermore, localized zones of the alluvial aquifer may also be affected by shallow saline water contaminations. These features of the hydrogeological system, which represent the main geophysical targets of the study, are all related to low-resistivity volumes and may show similar electrical resistivity values. This could generate vertical and lateral detectability issues in identifying such hydrogeological bodies. A further issue could arise from the fact that shallow saline water contaminations within the alluvial aquifer may not have a main orientation as occurs, for example, along structural discontinuities. For this reason, the VLF-EM method, unlike electrical resistivity methods, may not be able to detect such features.

For this purposes, we have tested and compared rapid and cost-effective surveys (VLF-EM) undertaken over the entire investigated area for an expeditious assessment of buried conductive bodies that could be connected to the saline water uprising and more detailed and accurate investigations (1D-4D electrical resistivity) to characterize restricted areas. These geophysical surveys were undertaken at the alluvial aquifer of the Oltrepò Pavese plain sector (Po Valley, Northern Italy). At the investigated test site, the alluvial aquifer is strongly conditioned by the presence of an important tectonic discontinuity, the "Vogherese Fault", a tectonic discontinuity buried below a few tens of meters of alluvial deposits. This is responsible for the sudden deepening towards the north that affects the hydrogeological bedrock (substratum) and is also responsible for the uprising of deep, saline paleo-waters. These Sodium Chloride (Na-Cl) rich waters rise along the discontinuities (faults, fractures) in the hydrogeological bedrock and flows into the overlying alluvial aquifer. This particular setting conditions the distribution of saline waters into the alluvial aquifer. They are evident in the southern sector of the plain, where the thickness of the aquifer is lower and so the dilution power of the fresh ground waters is reduced. This contamination prevents the exploitation of the aquifer, not only for drinking water supply, but also for agricultural and industrial use.

The origin of the Na-Cl rich waters is connected to the brines (very high density fluids) that are remnants of evaporated marine waters in the late Messinian (Late Miocene), trapped at the bottom of the Po plain aquifer (Conti et al., 2000). The occurrence of tectonic discontinuities within the hydrogeological bedrock allows the meteoric waters first to infiltrate and leach brines, then rise towards the shallow aquifer. According to some authors (Nanni and Zuppi, 1986; Conti et al., 2000) even the compressive forces that act along the Po Valley margins can squeeze the brines from the marine deposits, causing this uprise of saline waters. Pilla et al., 2010 showed that contamination from saline waters is not spatially and vertically homogeneous within the alluvial aquifer as highlighted by the hydrochemical investigations. Early results on the study of the saline water uprising occurring in the Oltrepò Pavese plain aquifer have been reported by Bersan et al. (2010) and Pilla et al. (2010).

This study may provide further insights into the applicability and effectiveness of electrical resistivity and electromagnetic methods in the investigation of similar, complex hydrogeological contexts where the aquifer's contamination by saline water is caused by mixing of freshwaters with brines, as it happens, for example, in the European countries Belgium, Denmark, England, Estonia, France, Italy, Spain (Darling et al., 1997; Desiderio and Rusi, 2004; Dever et al., 2001; Hinsby et al., 2001; Bonnesen et al., 2009; Marandi and Vallner, 2010), in Kansas and Texas in the USA (Stueber et al., 1998) or where the fossil salt waters, located different kilometres far from the coastline, are remainder of ancient marine ingressions, as for example in Togo, Morocco and Vietnam (Akouvi et al., 2008; Bouchaou et al., 2009).

2. Very Low Frequency Electromagnetic (VLF-EM) method

The theory that underlies the Very Low Frequency Electromagnetic (VLF-EM) technique is well described in the literature (Paterson and Ronka, 1971; Phillips and Richards, 1975; Ramesh Babu et al., 2007). The VLF-EM technique is a passive method that uses radiation from worldwide ground-based military radio transmitters used for navigation operating in the VLF band (15–30 kHz) as the primary electromagnetic (EM) field. These transmitters generate plane EM waves that can induce secondary eddy currents, particularly in electrically conductive elongate 2-D targets.

The VLF-EM is based on the measure of the vertical (*Hv*) and horizontal (*Ho*) components of the secondary field generated by lateral changes in conductivity in earth materials. Herein, that part of the vertical field which is in-phase with the horizontal field is called the 'in-phase component'; that part which is out-of-phase with the horizontal magnetic field is called the 'out-of-phase (quadrature) component'. VLF-EM profiles and maps are typically returned in terms of vertical (*Hv*) to horizontal (*Ho*) magnetic components *Hv/Ho*, termed dip-angle data. The presence of a well coupled (i.e., the structure must be roughly aligned towards the transmitter) conductive body such as fractures and faults is related to high *Hv/Ho* values. VLF-EM anomalies produced by water-bearing fractures may be very similar to those produced by moist, clay-filled, sealed fractures (Beard and Lutro, 2000). Larger anomalies are expected for saline water-bearing fractures.

VLF-EM has been widely used to prospect for conductive mineral deposits (Paál, 1965). However, it has been also used for rapid near-surface geological mapping (Gnaneshwar et al., 2011; Parker, 1980; Phillips and Richards, 1975; Saydam, 1981; Ramesh Babu et al., 2007; Sundararajan et al., 2006).

3. Electrical resistivity methods

Electrical resistivity methods are based on the estimation of the electrical resistivity of the subsoil and consist in the application of direct current into the ground by means of two current electrodes and the measure of the resulting voltage via two potential electrodes. The depth of investigation depends on the distance between the current electrodes. The arrangement of current and potential electrodes during the measurement is dependent on the chosen electrode array.

Most frequently used arrays are the dipole–dipole, Wenner, Schlumberger and pole-dipole arrays (e.g., Kneisel, 2006; Schrott and Sass, 2008). The dipole–dipole (DD) array uses two current electrodes on one side and two potential electrodes on the other side. This method is especially suitable for the detection of vertical structures as it shows high lateral resolution. Main disadvantages are sensitivity to high near-surface resistivity (Szalai and Szarka, 2008). The Wenner (W) array comprises four equally spaced electrodes deployed in a line in which potential electrodes are located between current electrodes. The method is especially suitable for the detection of horizontal structures (e.g., layering) as

it shows high vertical resolution. Disadvantages comprise shallower penetration and less subsurface information in comparison with the dipole–dipole array (Szalai et al., 2009). The Schlumberger (S) configuration is similar to the Wenner array; potential electrode spacing is constant but current electrode spacing is logarithmically increased. The method is especially appropriate for the detection of horizontal structures since it shows high vertical resolution like the Wenner array. The pole-dipole (PD) array is similar to the dipole–dipole array, but a current electrode, termed remote electrode, is so far away ("infinite" distance) that its location has negligible effect on the measurements. This array shows high lateral resolution and penetration depth and, even if it is more susceptible to noise contamination, may present a good compromise between resolution and signal strength (Smith, 1986). To obtain a true resistivity model of the subsurface an inversion procedure is needed (Loke and Barker, 1996).

The three main methods of electric resistivity surveys are Resistivity Depth Sounding (RDS), Resistivity Profiling (RP), and electric imaging, commonly termed Electrical Resistivity Tomography (ERT).

In the Resistivity Depth Sounding (RDS), electrode spacing is progressively expanded to increase the depth of investigation and measure vertical resistivity variations. Differently, in the Resistivity Profiling (RP), a constant electrode spacing is selected that senses the subsurface to the depth of interest, and this constant array is moved along a profile to measure lateral resistivity variations. Electrical Resistivity Tomography (ERT) provides an imaging of the subsurface electrical resistivity pattern and allows identifying subsurface structures. In ERT, which is based on a multi-electrode system, each of the electrodes alternatively acts as a current and potential electrode. Its theory (cf. Arato et al., 2014; Athanasiou et al., 2007; Buvat et al., 2013; Dahlin and Loke, 1998; Daily and Owen, 1991; Loke et al., 2003; Spiegel et al., 1980) and application (cf. Cassiani et al., 2009; Daily et al., 1992; Griffiths and Barker, 1993; Guérin and Benderitter, 1995; Guérin et al., 2004; Kuras et al., 2009; Ritz et al., 1999; Torrese, 2020) are well-documented in geophysical literature.

Electrical resistivity methods allow characterizing the subsurface materials in terms of their electrical properties. Changes in electrical resistivity correlate with variation in solid material, water saturation, fluid conductivity and porosity, which may be used to map stratigraphic units, geological structure, fractures, cavities, groundwater and anthropogenic structures. Electrical resistivity methods are well-suited techniques to identify and map low-resistivity structures as fine-grained alluvial layers (e.g., clayey and silty cover deposits), clayey or marly bedrocks (aquiclude) or saline water contaminations, as well as high resistivity structures, as coarse-grained alluvial layers (e.g., sands and gravels) or fresh water saturated alluvial deposits.

The resistivity signature of different hydrogeological bodies depends on the size of the target in relation to its depth and on the contrast between the resistivity of the target and that of the surrounding (host)

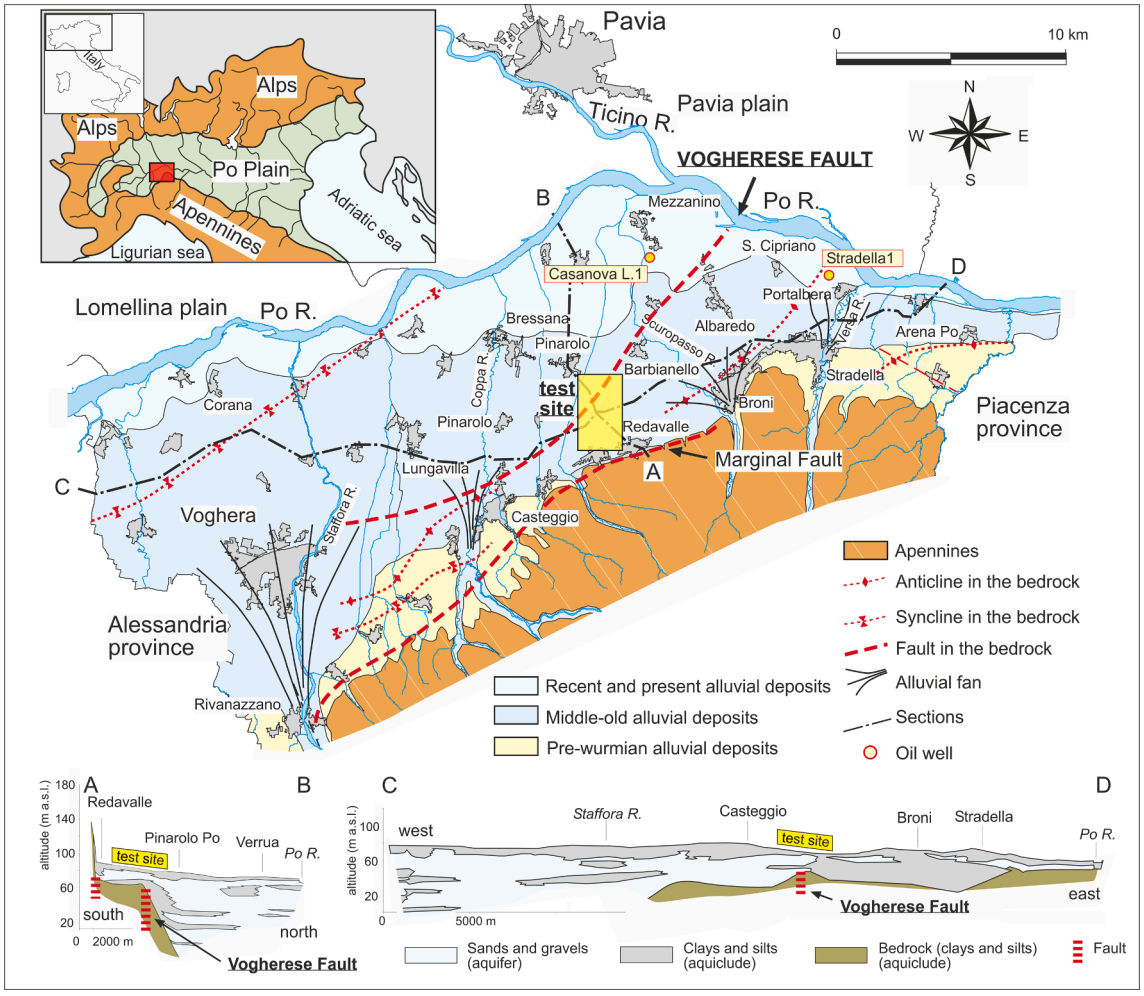

Fig. 1. Geographical and geological setting of the test site (Oltrepò Pavese plain sector) with hydrogeological sections (simplified from Cavanna et al, 1998). At the investigated test site, the alluvial aquifer is strongly conditioned by the presence of an important tectonic discontinuity, the Vogherese Fault. This is responsible for the sudden deepening that affects the hydrogeological bedrock (sections). The uplifment of the bedrock to the south-east of the Vogherese Fault (sections) is related to the Apennines uplifment.

rock. The amplitude of resistivity anomalies is an inverse function of the distance between the measurement points and the target. The deeper the target, the lower the reliability for the method in identifying it. The depth of investigation, the vertical and horizontal resolutions of electrical resistivity surveys are linked to: i) the electrode spacing, ii) the configuration array, iii) the quadrupole sequence, iv) the signal-to-noise ratio (S/N) ratio, v) the contrast between the resistivity of the target and the surrounding rock and/or background resistivity.

4. Geological and hydrogeological setting of the test site

The test site is located in the Oltrepò Pavese plain sector (Po Valley, Northern Italy) (Fig. 1). This sector is geologically characterized by alluvial quaternary deposits that cover Miocene–Pliocene marine deposits with very low hydraulic conductivity, formed by sandy-marls, sandstones, conglomerates, gypsum-rich marls and calcareous marls (Pellegrini and Vercesi, 1995).

The upper quaternary sediments, mainly deposited by the action of Po River and Apennine streams (Fig. 1), represent the main water-bearing units of the area. Three different hydrogeological units can be defined within the quarternary deposits: pre-würmian (>115 ky BP) alluvial deposits, middle-ancient alluvial deposits, recent and present alluvial deposits (Cavanna et al., 1998; Pilla et al., 2007) (Fig. 1). Only the latter two hydrogeological units are affected by the presence of Na-Cl rich waters. The middle-ancient alluvial deposits occupy most of the Oltrepò Pavese plain sector and are formed by alternating sand and gravel, with interbedded clays or clayey silts. The recent and present alluvial deposits, distributed mainly along the Po River, were originated by the post-würmian (<11.7 ky BP) depositional activity of this river. The most important Apennine streams also contributed to the deposition of these alluvial deposits.

The constant presence of a clayey silty covering, which has a varying maximum thickness of between 10 and 15 m, in the sectors close to the Apennine margin, and a minimum of 2 m, in the meandering area of the Po River, limits infiltration and influences the aquifer recharge, that occurs in correspondence of the coalescent fans originating from the deposition of Apennine streams (Pilla et al., 2007). Recharge contribution from the Po River must be excluded. In fact, groundwater flow direction is towards the Po River with the exception of occasional flooding events (Pilla et al., 2007). The aquifer is a single bedded unconfined aquifer, although it becomes locally and temporarily (during some periods of the year) confined due to the presence of the clayey silty covering.

The structural setting of the Oltrepò Pavese plain is strongly conditioned by the presence of an important tectonic discontinuity, known in literature as the Vogherese Fault (Boni, 1967) (Fig. 1). This fault has a NE-SW direction at a regional scale, from west of Casteggio to the Colle of S. Colombano (in the area of Pavia plain), passing across the confluence of the Ticino and Po rivers (Boni, 1967). Boni (1967), suggested that it is a normal fault with hanging wall to the NE, up to the Barbianello area. Here, it becomes an inverse fault to the south of Pinarolo, folding gradually towards west, north of Casteggio and Voghera. Given the absence of specific, recent studies on the subject, and since the definition of the fault type is outside the scope of this study, the Vogherese Fault has always been traced as a vertical fault on the cross-sections of this paper. The Vogherese Fault is responsible for the sudden deepening that affects the bedrock in the northern sector of the Oltrepò Pavese plain, and is also responsible for the strong variability on the thickness of the aquifer. The aquifer shows a thickness of a few meters in the southern sector, that represents the upper block, and hundreds meters in the northern sector, the lower block (Braga and Cerro, 1988; Cavanna et al., 1998; Regione Lombardia and ENI Divisione AGIP, 2002; AGIP, 1994) (Fig. 1).

There are two deep boreholes (depth up to ≈ 3 000 m) in the area that were drilled for oil exploration (Regione Lombardia and ENI Divisione AGIP, 2002). The Casanova Lonati 1 borehole (Fig. 1), which is located on the down-lifted block of the Vogherese Fault, intercepts the underlying marine origin deposits at a depth of 275 m. Brackish groundwater, which rises along the fault and flows into the continental deposits, is intercepted by the borehole at 136 m. Groundwater intercepts salt waters at 400 m (derived from self-potential and resistivity logs, as well as formation testing). Formation tests found sodium chloride up to a concentration of 34.4 g/l in the bedrock at depths of several hundred meters. The second borehole, the Stradella 1 borehole (Fig. 1), which is located on the up-lifted block of the fault, intercepts the underlying marine deposits at a depth of only 36 m.

This particular setting facilitates the uprising phenomenon of saline waters which shows itself at its best in the southern sector of the plain where the aquifer is thinner. Here the Na-Cl rich waters cannot be diluted by the more abundant calcium-bicarbonated groundwaters. This outlined setting strongly influences the chemistry of groundwater. The uprising of saline waters is also facilitated by structural discontinuities localized in the bedrock of marine origin. These discontinuities represent preferential flow paths for the saline waters and facilitate the flow towards the alluvial aquifer. This is demonstrated by the chloride distribution within the groundwater (Cameron et al., 2018; Pilla et al., 2007, 2010).

The existence of these mineralised waters in the Oltrepò Pavese area is well known since Roman times. In fact, the waters were (and still are) exploited for thermal purposes (S. Colombano al Lambro, Miradolo Terme, Salice Terme and Rivanazzano Terme are the most famous Spa centres located near the investigated area). However, this contamination may prevent the exploitation of the aquifer, not only for drinking water supply, but also for agricultural and industrial use.

4.1. Hydrochemical facies of groundwater

Two main hydrochemical facies can be identified within the Oltrepò Pavese groundwater: a calcium-bicarbonated hydrofacies, which characterises most of the groundwater of the alluvial aquifer; a sodium-chloride hydrofacies, which locally characterises the groundwater in some sectors of the area along the Vogherese Fault (Bersan et al., 2010; Pilla et al., 2007, 2010).

The calcium-bicarbonated hydrofacies has low to medium mineralisation with electrical conductivity (EC) values ranging between 800 and 1 200 μS/cm (Total Dissolved Solids (TDS) ranging between ≈550 mg/l and ≈850 mg/l). It is characterised by chlorides that do not exceed 100 mg/l; concentrations of bicarbonates vary between 300 and 700 mg/l, calcium varies between 50 and 200 mg/l, magnesium varies between 30 and 50 mg/l and sulphates vary between 30 and 100 mg/l (Pilla et al., 2010).

The sodium-chloride hydrofacies has a significantly higher mineralisation but extremely variable over the area with EC values that can be above 12 000 μS/cm (above ≈8 400 mg/l TDS), and are on average between 2 000 and 4 000 μS/cm (TDS ranging between ≈1 400 mg/l and ≈2 800 mg/l). The EC values are related to the solubilised chloride and sodium given that the concentrations of other major ions are relatively similar to those of the calcium-bicarbonated water described earlier. The variability of the Na-Cl groundwater is associated with the different degrees of mixing between the shallower fresh groundwater and the deeper saline waters (brines of the Po Plain). No correlation was observed between the variation in the degree of salinity of the water and the piezometric level of the groundwater.

Dissolution of gypsum-rich marls in the Miocene–Pliocene formations may have contributed in part to the sulphate concentration in the groundwater. As these formations are of marine origin, dissolution of these units could also account in part for the increased concentrations of sodium-chloride in the groundwater.

Hydrochemical investigations have shown three areas along the Vogherese Fault where the phenomenon seems to be more intense and widespread (Fig. S1 in the Supporting Information, Fig. 1): the test site area (to the west of Barbianello) where the highest concentrations

(above 4 000 mg/l) of chlorides were recorded, the sectors that includes Mezzanino and Albaredo Arnaboldi, where chloride concentrations can reach 3 000 mg/l, and finally, the area to the north of Casteggio where the chlorides can exceed 12 000 mg/l.

While the distribution of the sodium-chloride groundwater is controlled by the trend of the Vogherese Fault at a regional scale, higher variability in the distribution of the saline groundwater is observed at a local scale within the test site.

5. Materials and methods

5.1. Data collection

During the campaign a variety of geophysical surveys and experimental setups were tested. The study involved both investigations to explore a long transect (Fig. 2a), and detailed investigations to characterize a restricted area (Fig. 2b). One-dimensional (1D) to four-dimensional (4D) electrical resistivity and Very Low Frequency Electromagnetic (VLF-EM) surveys were acquired at the test site along a transect approximately 3 000 m long, along the "Strada Provinciale delle Saline" ("Salt Pan Provincial Road"), crossing the fault zone in a N-S direction and along a shorter profile transversal to it (Fig. 2).

A Very Low Frequency Electromagnetic (VLF-EM) profile (VLF-EM_29, Fig. 2) 2 200 m in length was acquired in October 2010, crossing the fault zone in a N-S direction.

Four Resistivity Depth Soundings (RDS_1-4, Fig. 2) were acquired in August 2009 (RDS_1-3) and in June 2010 (RDS_4) along roughly E-W profiles. A Schlumberger array was used with maximum AB/2 of 147 m, 215 m, 410 m and 180 m for RDS_1-4, respectively.

A Resistivity Profiling (RP_1, Fig. 2) 2 160 m in length was acquired in July 2009, crossing the fault zone in a N-S direction and overlapping to VLF-EM_29. A gradient array with aligned electrodes was used. Two to six measurements were acquired for each section with current electrode spacing AB = 80 m and potential electrode spacing MN = 10 m.

Five 2D Electrical Resistivity Tomography (ERT) (ERT_1-5) were acquired in July 2010 along an approximately 2 600 m long transect crossing the fault zone and partially overlapping to VLF-EM_29 and RP_1 (Fig. 2). Another ERT (ERT_6) was acquired in June 2014 at a transversal angle to the transect. Each profile is 470 m in length and was obtained using 48 electrodes spaced 10 m apart.

ERT_1-5, which are part of the surveys involved to explore the long transect, were collected using a 758 Wenner-Schlumberger (WS) array quadrupoles. ERT_6, which is part of the surveys involved to characterize a restricted area (detailed investigations), was collected using a 564 Wenner-Schlumberger (WS) array quadrupoles and a 570 Pseudo-Pole–Dipole (PsPD) array quadrupoles. The PsPD array comprised a remote electrode at a distance of 440 m from the profile and at a transversal angle to it. It was not possible to set the remote electrode at an "infinite" distance (for this reason it has been termed Pseudo-Pole–Dipole rather than Pole–Dipole). A hybrid (H) array sequence comprised of 1 134 measurements was developed by the combination of WS and PsPD array sequences.

Four three-dimensional (3D) ERT (3D_ERT_1-4) surveys were acquired between 2010 and 2015 (Fig. 2). 3D_ERT_1 and 3D_ERT_2 data were collected in July 2010 and September 2010, respectively. ERT_3 and ERT_4 data collection was undertaken in June 2013 and repeated in May 2015 to carry out a time-lapse (4D) analysis. A surface snake grid comprised of 12 × 4 electrodes spaced 10 m apart both along the X and Y axes was used. A sequence comprising 270 quadrupoles, using all feasible X, Y and diagonal dipole–dipole array configurations was used.

A WADI instrument by ABEM was used for acquiring all EM data. A fully automatic multi-electrode resistivity meter SYSCAL Jr Switch-48 by

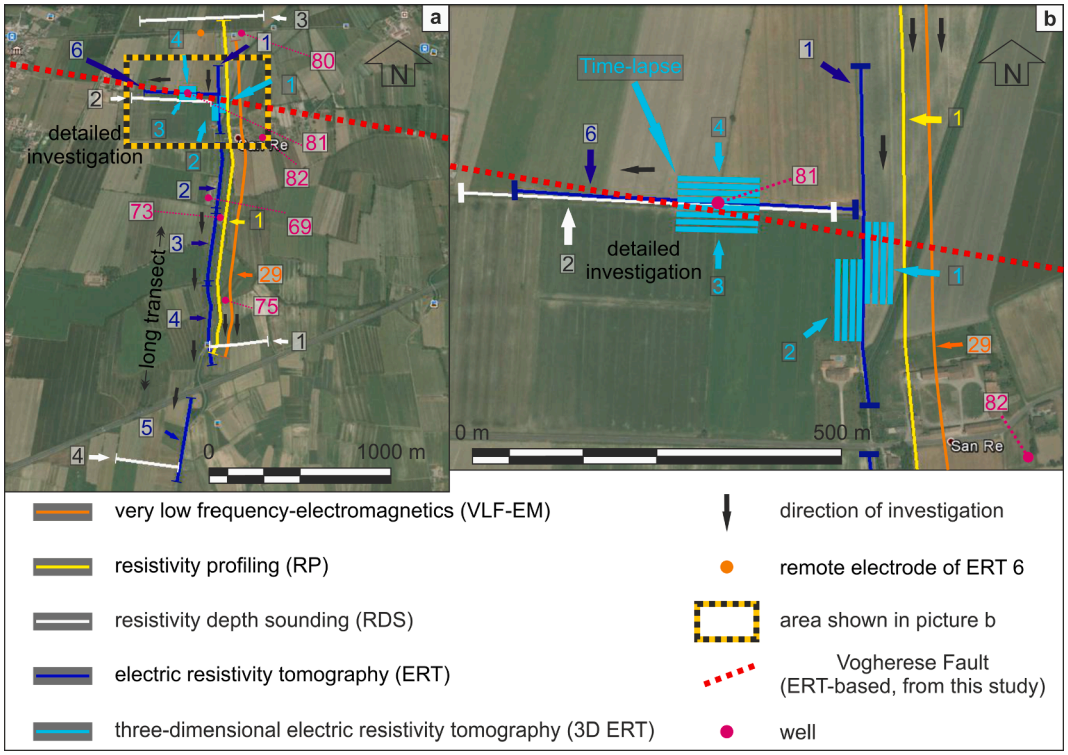

Fig. 2. (a) General and (b) detailed survey map of the test site (enlargement of the area included in the yellow-black dashed rectangle shown in (a). Maps in (a) and (b) also show the Vogherese Fault trace based on ERT surveys. (For interpretation of the references to colour in this figure legend, the reader is referred to the web version of this article.)

IRIS Instruments (400 V max output voltage, 1 200 mA max output current, 100 W max output power, http://www.iris-instruments.com/syscal-juniorsw.html), was used for acquiring all electrical resistivity data.

Given the presence of an extremely variable groundwater mineralisation over the area, we carried out EC measures rather than Total Dissolved Solids (TDS): in such a context, EC is especially suitable for the differentiation between calcium-bicarbonated and sodium-chloride hydrofacies. However, it is worth pointing out that TDS is preferable in presence of a lower variability in water mineralization since, for example, calcium-bicarbonated waters show a lower EC than sodium-chloride waters with similar TDS.

A Pasi BFK 100 hydrostatic probe was used for measuring piezometric levels, a WTW Cond 3401 conductivity meter was used for acquiring electrical conductivity and temperature data and a WTW pH 340/ion was used for acquiring pH and Redox potential data. Groundwater sampling from the wells was carried out with a Cellai 504S peristaltic pump. Major ions were analyzed in the laboratory of Università di Pavia with a Dionex DX 120 chromatograph, while volumetric analysis was used for the determination of alkalinity.

5.2. Data processing and inversion

A Fraser filter (Fraser, 1969, 1981) was used to provide a simple scheme for semi-quantitative interpretation of Very Low Frequency

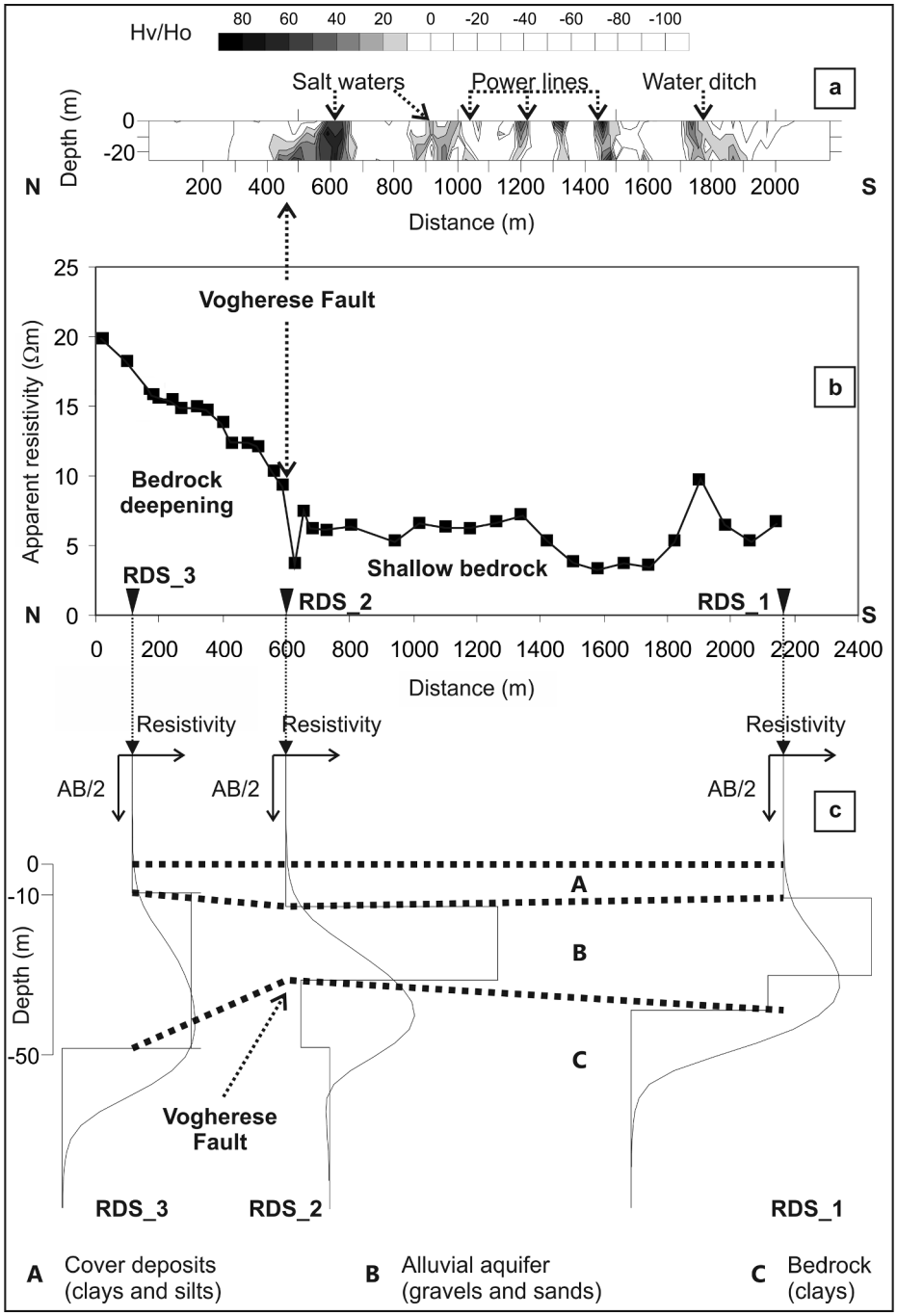

Fig. 3. Long transect: (a) electromagnetic pseudo-section (*Hv/Ho*) of the real part (positive values) obtained through a Fraser filter applied to VLF-EM_29 profile; (b) Resistivity Profiling RP_1 obtained through gradient array with AB = 80 m, MN = 10 m; (c) Resistivity Depth Soundings RDS_1, RDS_2, RDS_3 and resulting electro-stratigraphic section. Figure modified from Pilla et al., 2010.

Electromagnetic (VLF-EM) data and obtain the equivalent current densities (Ogilvy and Lee, 1991; Sundararajan et al., 2006) at a constant depth which would cause a magnetic field. If $f(i) = fi$ represents the collected data so, *f1, f2, f3 and f4* represent four equal spaced consecutive dip-angle (*Hv/Ho*) readings and ∇x represents the space between each station along the profile,

$$\frac{(f1+f2)-(f3+f4))}{\nabla x} \quad (1)$$

is the Fraser filter of those four values. Since ∇x is constant, it can be ignored and the Fraser filter considered to be

$$(f1+f2)-(f3+f4) \quad (2)$$

The use of this filter allows a reduction of noise through a low-pass filter and the removal of the asymmetry inherent in dip-angle data.

The magnitudes of the currents that would have to flow at different depths to produce a given anomaly have been obtained through this filter applied for different measured intervals $n\cdot\nabla x$, with $n = 1, 2, 3, 4, 5, 6$. Kriging geostatistical gridding methods have been used to interpolate the filtered values and achieve the section shown in Fig. 3a.

The depth of penetration P of the VLF-EM investigation can be estimated on average just over 20 m based on (3)

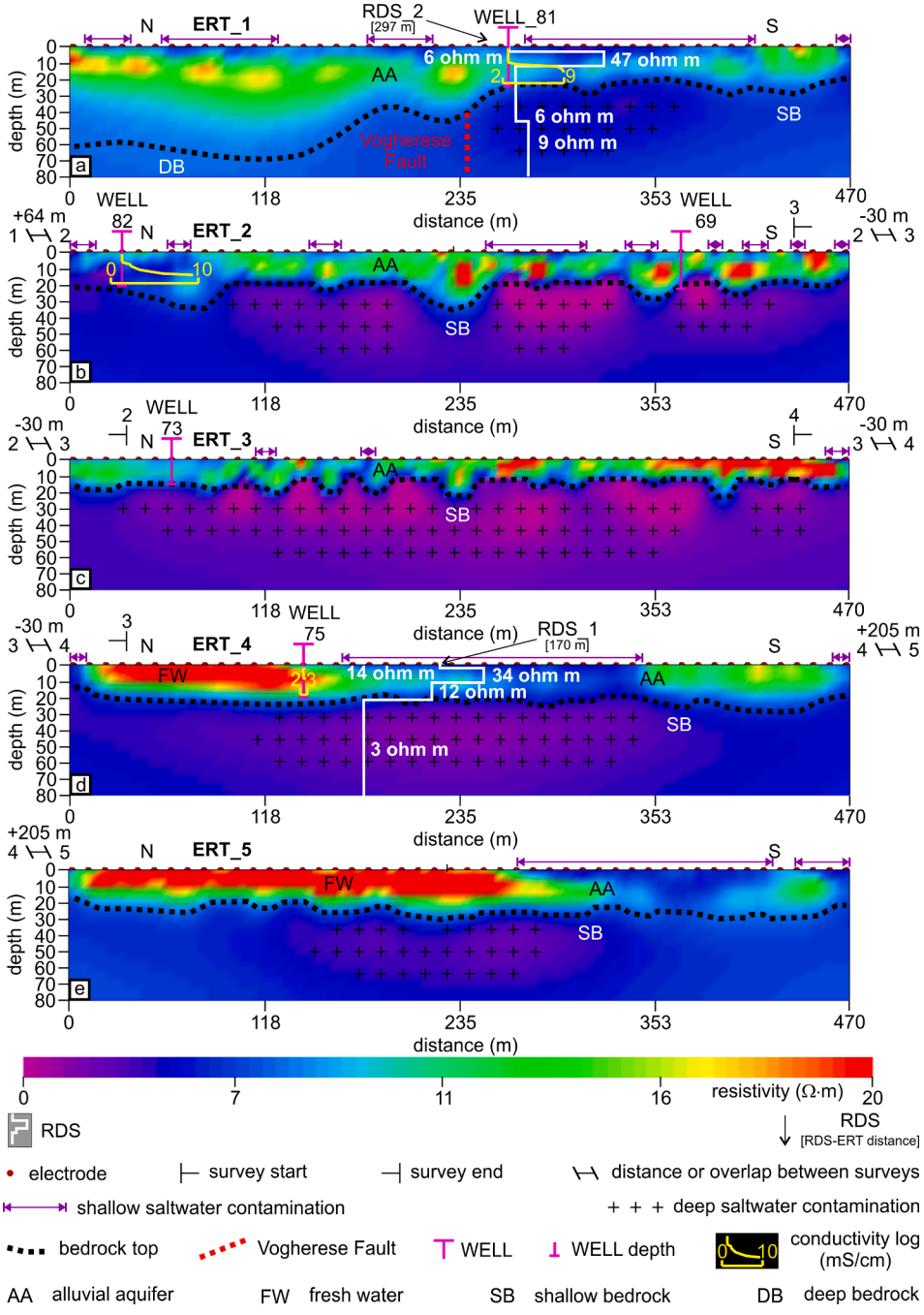

Fig. 4. Long transect: (a-e) transect (approximately 2 600 m long) ERT_1-ERT_5 (inverse resistivity sections) showing the geometry of the bedrock at the base of the alluvial aquifer, the Vogherese Fault trace localized on the basis of the ERT surveys, and the occurrence of localised and restricted zones of salinisation within the alluvial aquifer.

$$P = 500\sqrt{\frac{\rho}{f}} \quad (3)$$

with f = used frequency, ρ=average shallow resistivity obtained from electrical resistivity surveys.

Smoothing was not applied to Resistivity Profiling (RP) data (Fig. 3b). Inverse resistivity profiles from Resistivity Depth Soundings (RDSs) (Fig. 3c) were obtained through inversion of the experimental curve.

Electrical Resistivity Tomography (ERT) data required a more robust data processing and inversion. Data processing involved the removal of outliers from the apparent resistivity data. Some problematic data with unrealistically high standard deviation, high-resistivity and or negative resistivity (in 2D surveys) were all removed from apparent data.

Data inversion was performed using ERTLab Solver (Release 1.3.1, by Geostudi Astier s.r.l. - Multi-Phase Technologies LLC) based on tetrahedral Finite Element Modelling (FEM). As regards the Pseudo-Pole–Dipole (PsPD) array, the exact finite location (X, Y, Z coordinates) of the remote electrode was considered during data processing (Razafindratsima and Lataste, 2014; Robain et al., 1999) instead of the infinite location of the remote electrode provided for by theoretical Pole–Dipole (PD) array.

Tetrahedral discretization was used in both forward and inverse modelling. The foreground region was discretized using a 5 m cell size for all 2D and 3D ERTs, i.e., half the electrode spacing, to give the model high accuracy. The background region was discretized using an increasing element size towards the outside of the domain, according to the sequence: 1×, 1×, 2×, 4× and 8× the foreground element size.

The forward modelling was performed using mixed boundary conditions (Dirichlet-Neumann) and a tolerance (stop criterion) of 1.0E-7 for a Symmetric Successive Over-Relaxation Conjugate Gradient (SSORCG) iterative solver. Data inversion was based on a least-squares smoothness constrained approach (LaBrecque et al., 1996). Noise was appropriately managed using a data-weighting algorithm (Morelli and LaBrecque, 1996) that allows the variance matrix after each data point iteration that was poorly fitted by the model to be adaptively changed. The inverse modelling was performed using a maximum number of internal inverse Preconditioned Conjugate Gradient (PCG) iterations of 5 and a tolerance (stop criterion) for inverse PCG iterations of 0.001. The amount of roughness from one iteration to the next was controlled to assess maximum layering: a low value of reweight constant (0.1) was set with the objective of generating maximum heterogeneity.

The inverse resistivity models (Figs. 4–7, 10–12) were obtained by inverting the datasets acquired through single arrays, or by merging and jointly inverting datasets from different arrays which can deliver better detectability and imaging and, hence, provide more accurate inverse models (Szalai et al., 2009; Torrese, 2020) and more reliable ERT imaging (de la Vega et al., 2003; Seaton and Burbey, 2002). Inversion involved the application of homogeneous starting models that set at each node the average measured apparent resistivity value. The final inverse resistivity models were chosen based on the minimum data residual (or misfit error).

5.3. Cross-validation of geophysical results with well logs

The test site provided an ideal opportunity to cross-validate geophysical results with extensive ground truth. The study involved six shallow water wells for irrigational purposes, available at the site, WELL_69, WELL_73, WELL_75, WELL_80, WELL_81 and WELL_82 (Fig. 2). These wells were drilled prior to the present study, with destructive rotary or auger techniques until the top of the (impermeable) bedrock. All the wells are fully screened. Although no logs of chip samples are available and these wells do not provide accurate stratigraphic logs they still provide information regarding the depth to bedrock below alluvial deposits. WELL_69, WELL_73, WELL_75, WELL_81 and WELL_82 located in the S sector respect to the fault trace intercept the bedrock (Figs. 4–7); conversely, WELL_80, located in the N sector, does not intercept it.

Piezometric level measures, water sampling and analysis (major ions, Table S1 in the Supporting Information) and electrical conductivity (EC) logs have been undertaken within Well_75, WELL_81 and Well_82

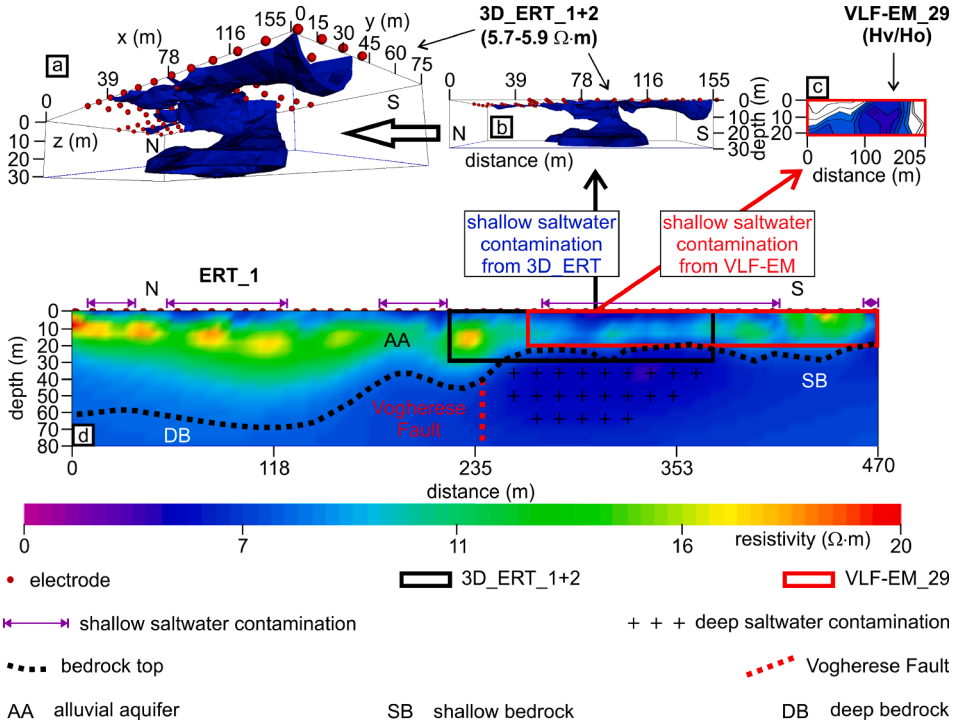

Fig. 5. Part of the long transect: (a, b) saltwater plume extraction from 3D_ERT_1+2 (combined inversion) inverse resistivity model with different perspective views; (c) saltwater plume extraction from VLF-EM_29; (d) ERT_1 (inverse resistivity section) showing the geometry of the bedrock at the base of the alluvial aquifer, the Vogherese Fault trace localized on the basis of the ERT survey, and the occurrence of localised and restricted zones of salinisation within the aquifer.

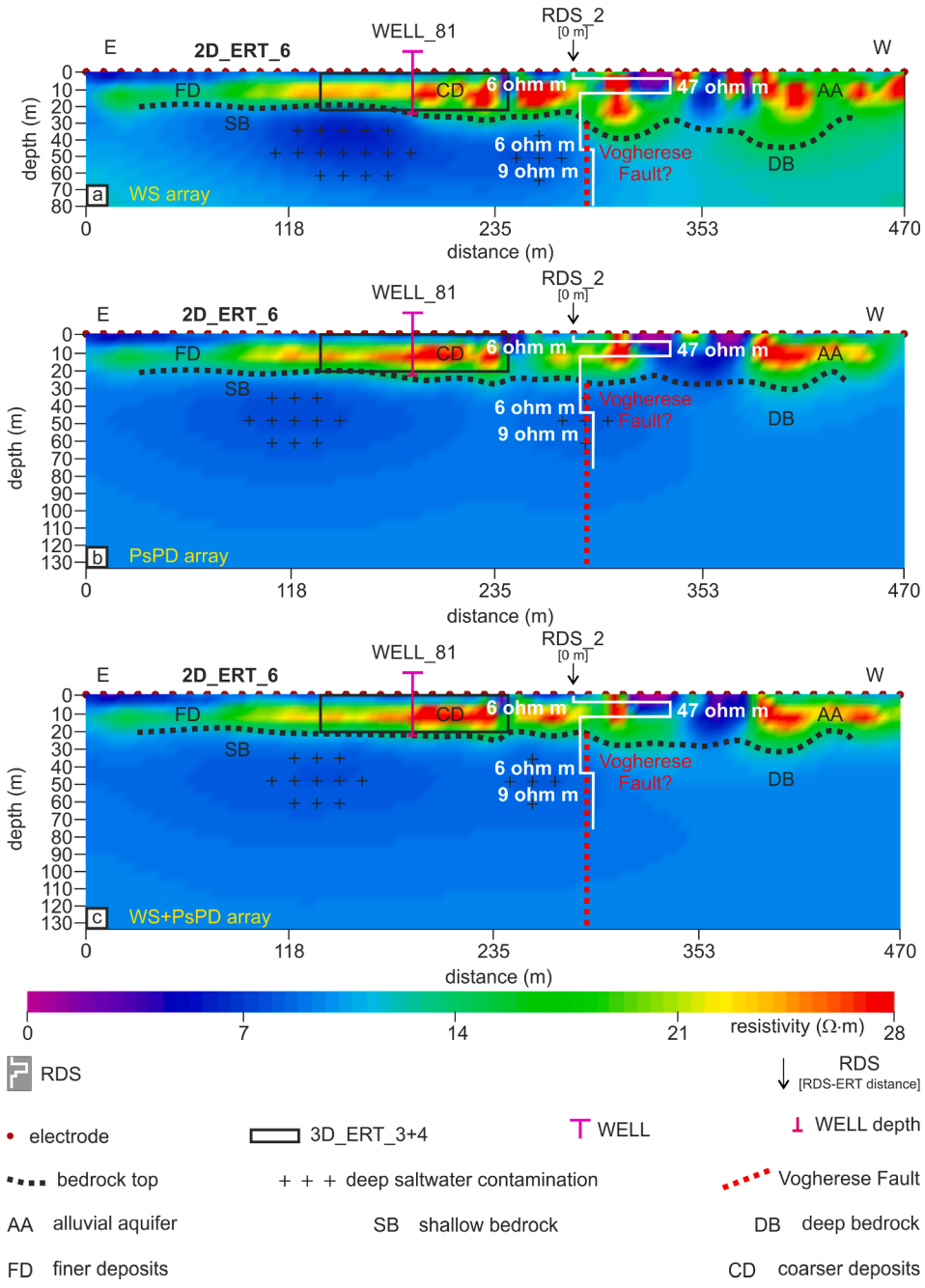

Fig. 6. Detailed investigation: comparison between the inverse resistivity sections of 2D_ERT_6 obtained by (a) WS, (b) PsPD and (c) H arrays, showing the occurrence of localized zones of salinisation within the bedrock.

(Fig. 4); piezometric level measures, water sampling and analysis (major ions), electrical conductivity, temperature and redox potential logs have been undertaken within Well_81 (Figs. 7, 9, 10, 11) (Pilla et al., 2010).

In this study water salinity was classified according to these classes: fresh water with EC < 500 µS/cm, slightly brackish water with EC ranging between 500 and 4 000 µS/cm, moderately brackish water with EC ranging between 4 000 and 8 000 µS/cm, highly brackish water with EC ranging between 8 000 and 12 000 µS/cm, saltwater with EC ranging between 12 000 and 70 000 µS/cm, brine with EC > 70 000 µS/cm (Table S2 in the Supporting Information). The term saline water was used to define a highly mineralized water, and includes both brackish water and saltwater.

Water sampling and electrical conductivity logs show an extremely variable mineralisation over the test site with EC changes up to 9 000 µS/cm (up to ≈6 200 mg/l TDS) (Fig. 4 and Fig. S2 in the Supporting Information). The variability of the Na-Cl groundwater is associated with the different degrees of mixing between the shallower fresh groundwater and the deeper saline waters.

Specifically, WELL_81 resistivity and temperature logs carried out the 5th June 2013 and the 4th July 2013, as well as the redox potential log carried out the 4th July 2013 are reported in Fig. 7. If analyzing in detail the resistivity log undertaken the 5th June 2013 which was used for the cross-validation of 3D and time-lapse (4D) geophysical surveys (Fig. 7), it can be found a transition between slightly brackish groundwater (1 430 µS/cm on average, ≈1 000 mg/l TDS, 1–10 m of depth, June 2013) to underlying moderately brackish groundwater (5 262 µS/

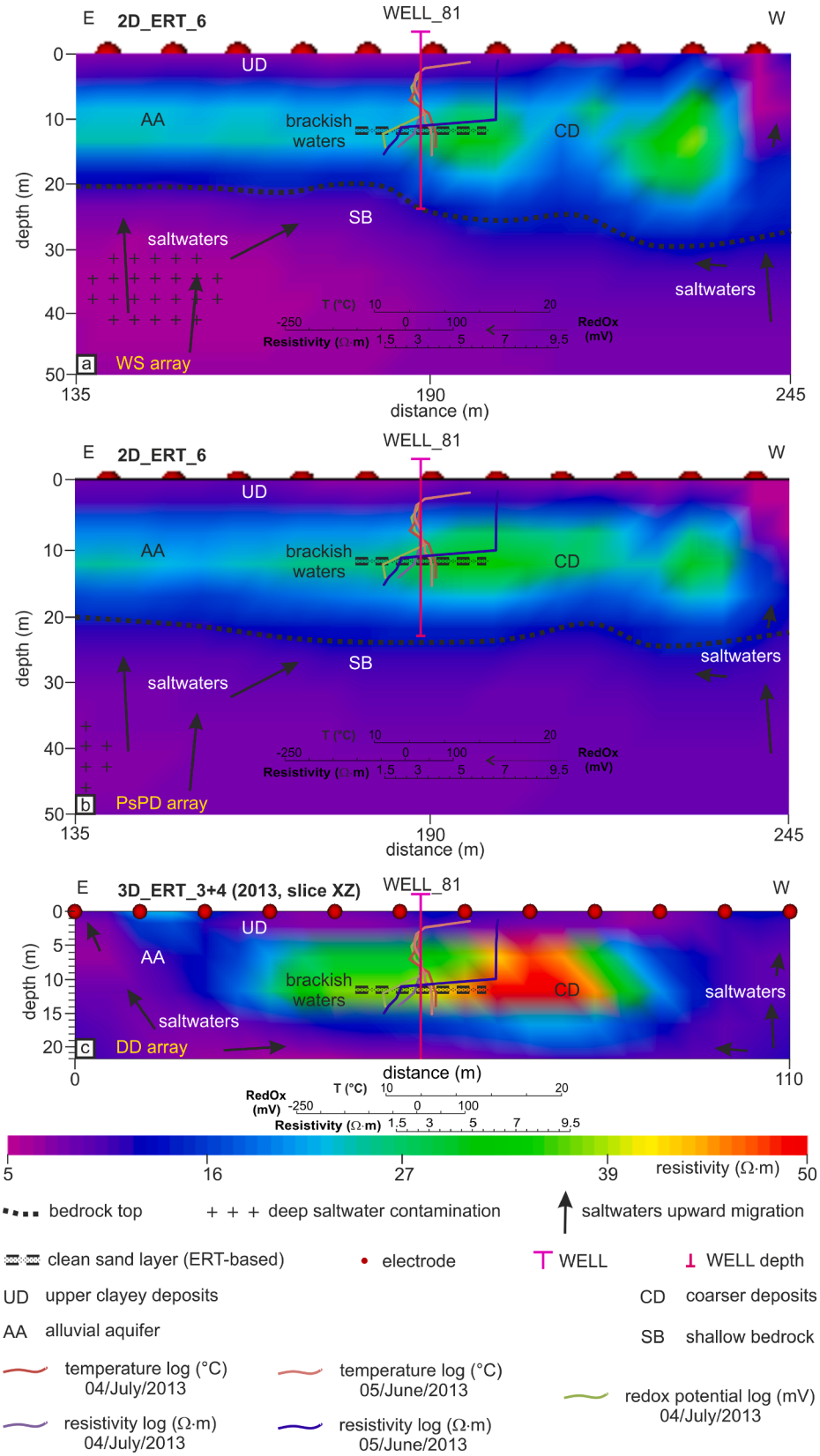

Fig. 7. Detailed investigation: comparison between narrow scale range extractions from 2D_ERT_6 (WS and PsPD arrays) and the overlapping XZ slice of 3D_ERT_3+4 (DD array). Well_81 logs clearly reveal the slightly to moderately brackish water interface that that seems to be localized in correspondence of a clean sand layer (Fig. 9) contaminated by moderately brackish water at an apparent depth between 11 m and 12 m. Clayey bedrock, upper clayey deposits and saltwater contaminations show very close resistivity values.

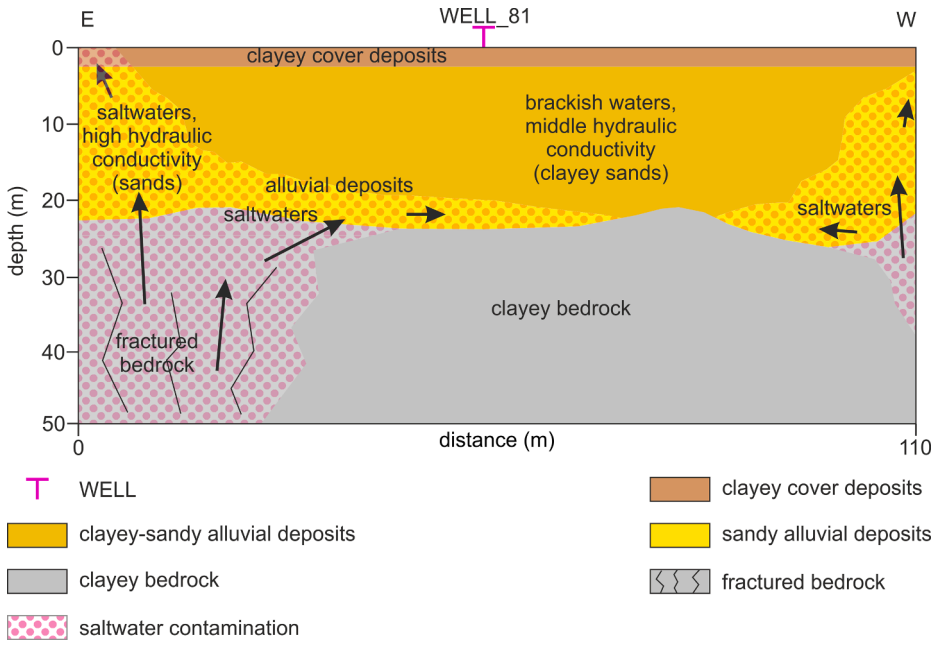

Fig. 8. Hydrogeological model derived from geophysical models 3D_ERT_3+4 (Fig. 7c) at shallow depths (where 3D ERT provides better accuracy) and 2D_ERT_6 (Fig. 7a, b) at greater depths; to compare also with Figs. 10 and 11. This hydrogeological model suggests that the distribution of saline water contaminations is a hydraulic conductivity-controlled process at the plume-scale within alluvial deposits.

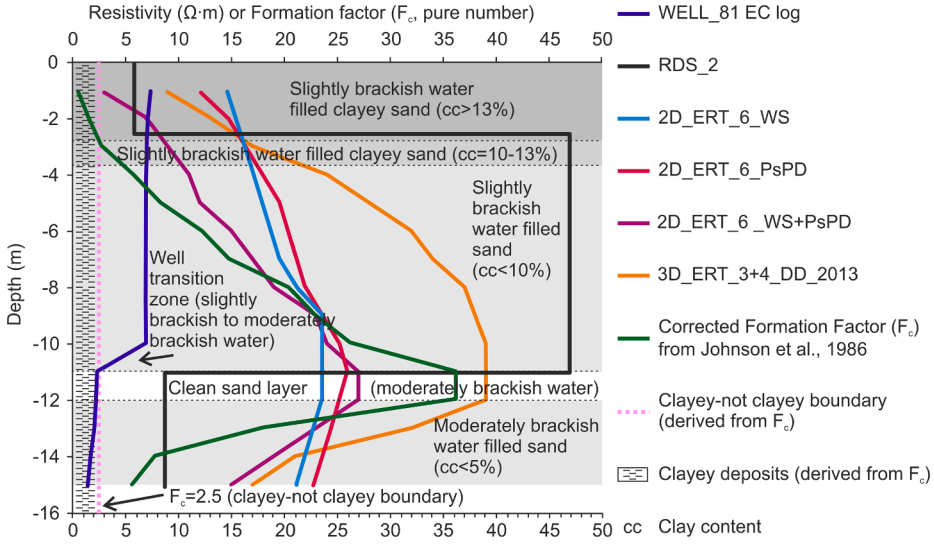

Fig. 9. Detailed investigation: comparison between vertical profiles extracted from a variety of 1D, 2D and 3D electrical resistivity surveys and experimental setups along WELL_81 axis and the resistivity log of Well_81. Formation factor-based parameterization suggests a decrease in clay content with depth, ranging from > 13% to < 5% with the exception of the presence of a clean sand layer between 11 m and 12 m of depth. Comparison between the electrical resistivity profiles along the well axis revealed that the higher is the accuracy of the geophysical method, the larger is the measured resistivity variation range: for example, 3D ERT (more accurate) and 2D ERT (less accurate) measured a resistivity range of 30 ohm·m and 15 ohm·m (on average), respectively; combined (hybrid) array WS + PsPD (maximum accuracy), PsPD array (middle accuracy) and WS array (minimum accuracy) measured a resistivity range of 23 ohm·m, 13 ohm·m and 9 ohm·m, respectively; RDS profile is not directly comparable as it relates to a much larger volume of subsoil.

cm on average, ≈3 700 mg/l TDS, 11–15 m of depth, June 2013) at 11 m depth. Likewise, the temperature log (5th June 2013, Fig. 7) shows a transition between shallower relative colder groundwater (an average temperature of 12.8 °C, 3–10 m of depth, June 2013) and deeper relative warmer groundwater (an average temperature of 13.5 °C, 11–15 m of depth, June 2013) at 11 m depth.

6. Results

6.1. The long transect revealing general hydrogeological setting

The greater anomaly identified along Very Low Frequency Electromagnetic VLF-EM_29 ("salt waters" at 400–680 m, Figs. 3a and 5c) is associated with a shallow saline water contamination, i.e., a conductive buried bodies, steeply-dipping and well coupled with the EM transmitter. This anomaly can be identified slightly south of a strong apparent resistivity variation along Resistivity Profiling RP_1 at 650 m ("Vogherese Fault", Fig. 3b). This identifies a change between two zones: the increase in apparent resistivity along RP_1 from approximately 7 ohm·m to 20 ohm·m towards the north from progressive meter 650 m to 0 m is indicative of the deepening of the bedrock (north of the Vogherese Fault). This is also consistent with Resistivity Depth Sounding (RDS) results which indicate a deepening of the bedrock from depth of 11 m (RDS_2) to depth of 47 m (RDS_3). The low apparent resistivity values towards the south from 2 160 m to 650 m (Fig. 3b) indicate a shallow depth of the bedrock (south of the Vogherese Fault). In particular, the apparent resistivity values along RP_1 in this area are essentially related to a qualitative description of the geometry of the bedrock. Although the latter remains at a shallow depth (11 m at 600 m as indicated by RDS_2 and 21 m at 2 160 m as indicated by RDS_1, Fig. 3c), the apparent resistivity values indicate local shallowing of the bedrock from 1 500 m to 1 750 m where the values are typical of the bedrock resistivity

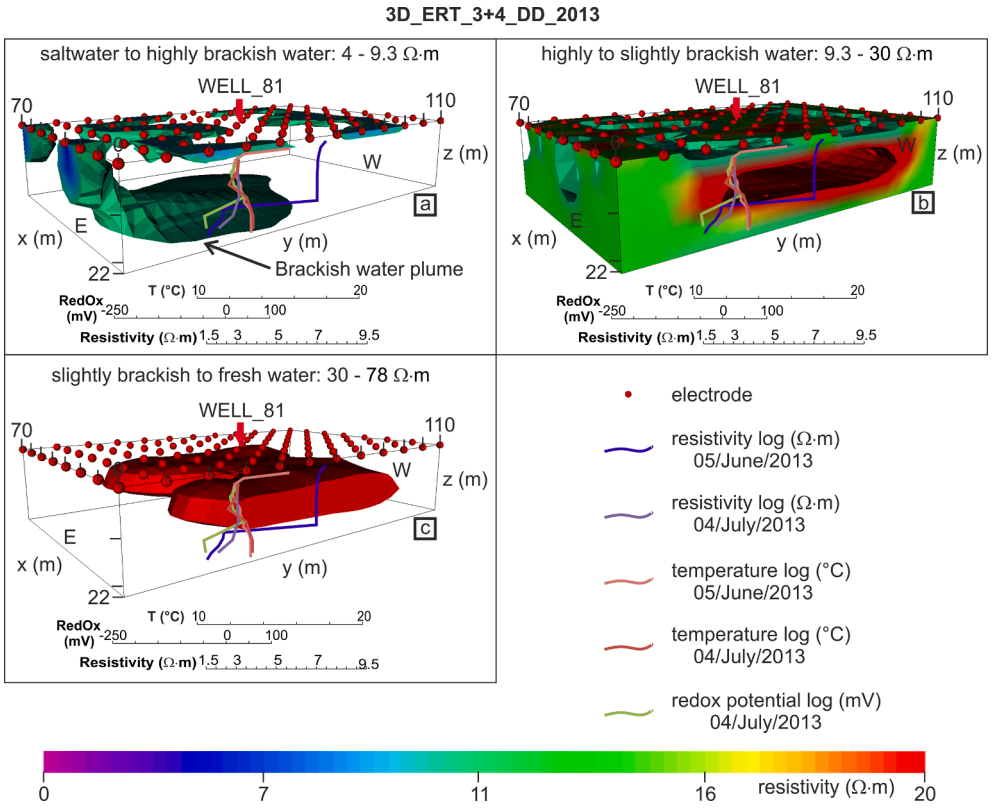

Fig. 10. Detailed investigation: deep salt waters reach the alluvial aquifer during upward migration, diffuse and mix with the fresh groundwater of the shallow aquifer, therefore originating different degrees of groundwater salinity within the aquifer; 3D_ERT_3+4 resistivity block obtained from the dataset collected the 3rd June 2013; (a) saltwater to highly brackish water plume contaminating a sandy body within the alluvial aquifer and shallow low resistivity anomalies within the upper clayey deposits; (b) highly to slightly brackish water contaminating clayey sandy deposits; (c) slightly brackish to fresh water contaminating clayey sandy deposits. The resistivity model shows good correlation with respect to WELL_81 logs which found at 11 m of depth a drop in resistivity, along with an increase of temperature and a decrease of redox potential of groundwater suggesting a well transition zone between slightly and moderately brackish water. To compare with Figs. 7c, 8 and 9.

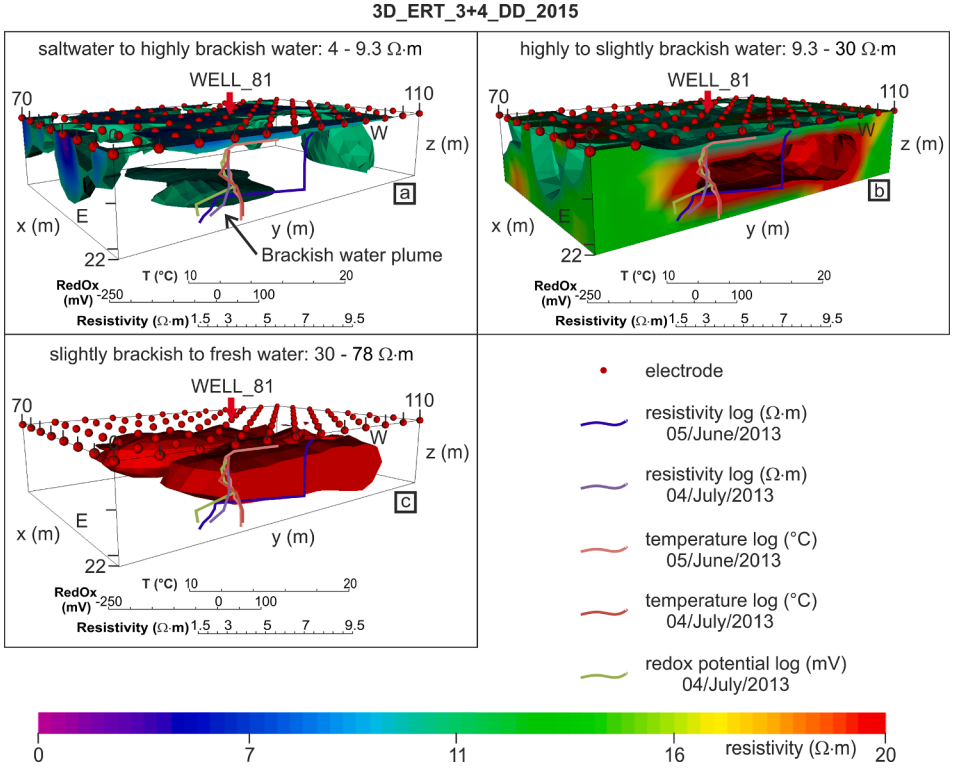

Fig. 11. Detailed investigation which shows different degrees of groundwater salinity within the aquifer: 3D_ERT_3+4 resistivity block obtained from the dataset collected the 20th May 2015; (a) to (c) bodies can be directly compared to bodies (a) to (c) shown in Fig. 10; a decrease in size of the (a) saltwater to highly brackish water plume and an increase in resistivity values of the alluvial aquifer during late spring of 2015 are likely due to 52% lower rainfall during spring 2015 with respect to spring 2013 (piston flow mechanism proposed by Re and Zuppi (2011)).

(3–4 ohm·m). Higher apparent resistivity values indicate a deepening of the bedrock at 1 900 m (Fig. 3b). These evidences allow to accurately localize the Vogherese Fault at the investigate site.

This hydrogeological configuration is confirmed by RDS_1-3 (Fig. 3c) which identify shallow bedrock to the south and the above mentioned deepening of the bedrock to the north and is also congruent with the

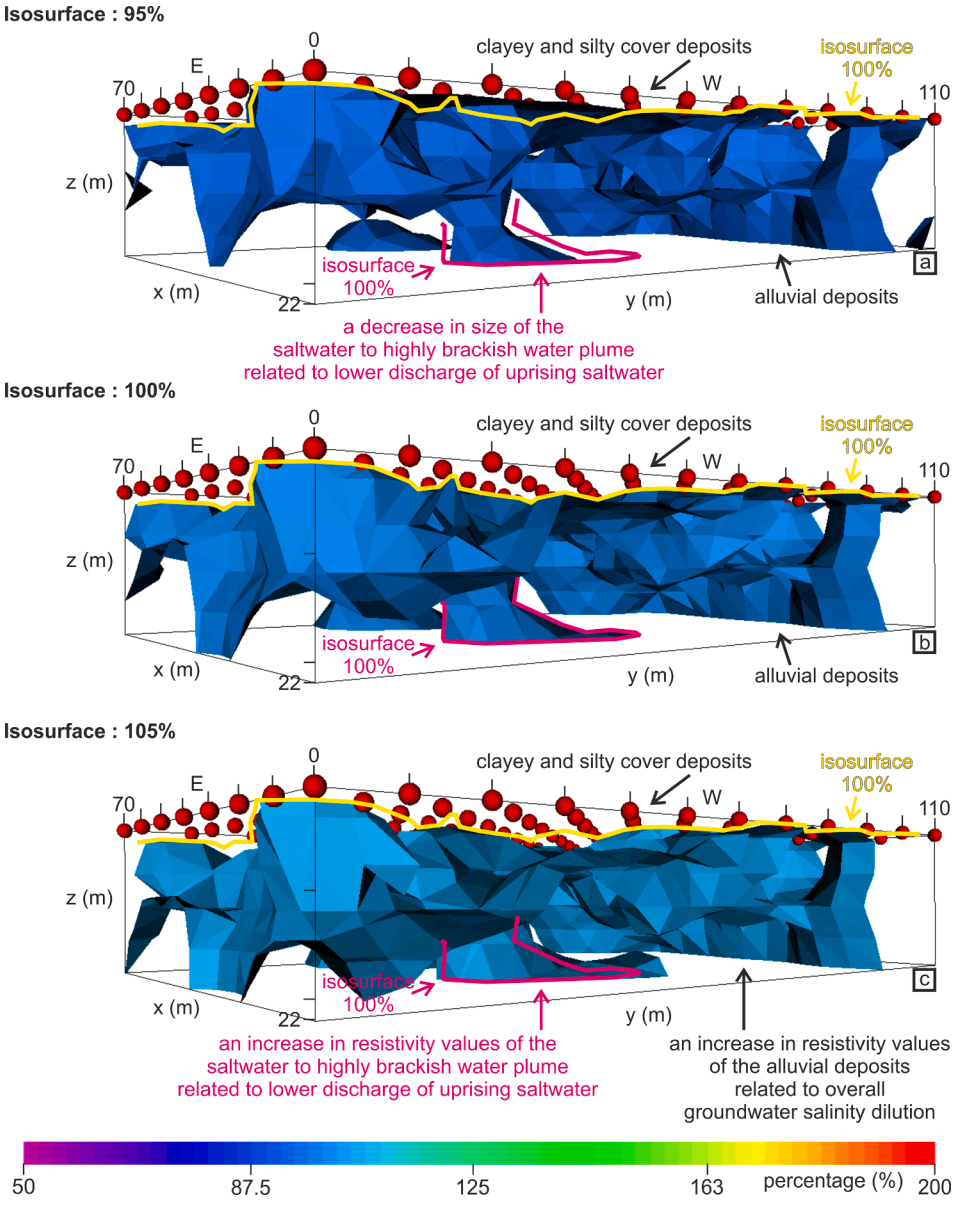

Fig. 12. Detailed investigation: time-lapse percentage ratio between the 2015 (Fig. 11) and 2013 (Fig. 10) resistivity block models; isosurfaces (a) 5% lower resistivity values, (b) consistent resistivity values, (c) 5% higher resistivity values. A decrease in size of the saltwater to highly brackish water plume and an increase in resistivity values of the alluvial aquifer during late spring of 2015 are likely due to 52% lower rainfall during spring 2015 with respect to spring 2013 (piston flow mechanism proposed by Re and Zuppi (2011)). A decrease in resistivity values of the clayey and silty cover deposits due to previous day rainfall has also been observed during late spring of 2015.

stratigraphic logs of the wells. Indeed, WELL_69, WELL_73, WELL_75, WELL_81 and WELL_82 located in the S sector respect to the fault trace intercept the bedrock (Figs. 4–7); conversely, WELL_80, located in the N sector, does not intercept it.

This hydrogeological setting based on VLF-EM, RP and RDS results is confirmed by more accurate and complete Electrical Resistivity Tomography ERT_1-5 and 3D_ERT_1+2 surveys (Figs. 4 and 5). In these inverse resistivity models, warm colours (from green to red) are associated with freshwater-saturated alluvial deposits (e.g., freshwater-saturated clayey-to-sandy deposits); cool colours (from purple to blue) are associated with clayey and silty cover deposits, saline water-saturated alluvial deposits (e.g., saline water-saturated sandy-to-gravelly deposits) or with the clayey bedrock (locally saline water-saturated).

The inverse models indicate sharp and irregular contact between the alluvial aquifer and the underlying hydrogeological bedrock. The hydrogeological bedrock (3–6 ohm·m) at the base of the alluvial aquifer (20–40 ohm·m) is characterized by morphological irregularities, which are likely to have been shaped either by tectonics (Vogherese Fault zone) and/or by the paleo-river's erosion. In the southern area of the investigated transect (south of the fault) the thickness of the aquifer varies between 10 m and 30 m (Fig. 4b–e). This depth increases northward due to the Vogherese Fault ("deep bedrock (DB)", Fig. 4a). These evidences are consistent with well observations regarding bedrock depth (Fig. 4). The bedrock is affected by saltwater contaminations which show resistivity values lower than 3 ohm·m. These contaminations are likely localized along structural discontinuities which represent preferential flow paths for the saline waters and facilitate the flow towards the alluvial aquifer.

The resistivity imaging obtained for the long transect, which was cross-validated with electrical conductivity logs, revealed an extremely variable mineralisation of the groundwater over the test site. Contamination-related low resistivity anomalies (cool colors within the aquifer) correspond to electrical conductivity values up to 9 000 μS/cm (up to ≈6 200 mg/l TDS) (e.g., WELL_81 and WELL_82 in Fig. 4 and Fig. S2 in the Supporting Information); high resistivity anomalies (warm colors within the aquifer) are found in correspondence of contamination-free zones (e.g.,

WELL_75, in Fig. 4). The variability of electrical resistivity with depth (Fig. 4) is associated with the different degrees of mixing between the shallower fresh groundwater and the deeper saline waters.

Both the 2D and 3D ERT surveys pointed out the existence of localised and restricted zones of salinisation within the aquifer. These zones show resistivity values ranging between 3 and 8 ohm·m (Fig. 4). Specifically, the aforementioned greater anomaly identified along VLF-EM_29 ("salt waters" at 400–680 m, Figs. 3a and 5c) corresponds to the shallow saline water plume extracted from 3D_ERT_1+2 (5.7–5.9 ohm·m, Fig. 5a,b). This is a detailed 3D imaging of the irregular-shaped shallow saltwater contamination within the alluvial aquifer.

In general, the groundwater salinity starts to increase at depths of between 5 and 8 m (e.g., WELL_75; WELL_81, WELL_82) (Fig. 4 and Fig. S2 in the Supporting Information). This can increase to depths of 10–15 m like in the case of WELL 81 (Figs. 7 and 9). In other cases, the depth is just below ground level like in some areas near the test site where saline waters were found in the surface drainage network which is buried in the first few meters of the drift deposits. The correlation between changes in the EC logs and changes in the ERT resistivity is not always observed if the wells are not located in correspondence with the geophysical surveys (well-ERT distance ranging between 80 m and 215 m, Fig. S2 in the Supporting Information). For example, the EC log of WELL_82 shows that the salinity starts to increase at a depth of 5 m, corresponding to a saltwater contamination within the alluvial aquifer revealed by ERT_2 (Fig. 4 and Fig. S2b in the Supporting Information). Otherwise, the EC logs of WELL_81 and WELL_75 show a change in conductivity unrelated to the change in resistivity of ERT_1 and ERT_4, respectively (Fig. 4 and Fig. S2a,c in the Supporting Information). This suggests an extremely variable mineralisation of groundwater over the test site. Correlation between changes in the EC log and changes in the ERT resistivity is observed between WELL_81 and ERT_6 and 3D_ERT_3+4 (Figs. 7 and 9). In this case the well is located in correspondence with the geophysical surveys.

6.2. Detailed investigation and time-lapse monitoring

Electrical Resistivity Tomography ERT_6, which was acquired at a transversal angle to the longer transect (Fig. 2), confirmed the hydrogeological configuration which shows a shallow bedrock to the east and a deepening of the bedrock to the west (Fig. 6) caused by the Vogherese Fault. ERT_6 results together with ERT_1 (Figs. 4a and 5d) results allowed achieving detailed localization and trace of the Vogherese Fault which appears to have an ENE-WSW orientation at the scale of the test site (Fig. 1b,c). In addition, ERT_6 confirmed the presence of restricted zones of the bedrock affected by saline water contaminations which are likely localised and restricted zones along structural discontinuities. Comparison between the imaging achieved by different arrays revealed that:

- the Wenner-Schlumberger (WS) array (Fig. 6a) showed higher vertical resolution and a tendency to enhance layering in identifying alluvial deposits and deep saltwater contaminations; furthermore, it showed larger signal amplitude but lower penetration depth;
- the Pseudo-Pole–Dipole (PsPD) array (Fig. 6b) showed higher lateral resolution (above all at depth) and more compact and vertically-extended bodies; furthermore, it showed greater penetration depth in delineating the two deep saltwater contaminations; even if this array is more susceptible to noise contamination, may present a good compromise between resolution and signal strength;
- the hybrid (H) array (Fig. 6c), developed by the combination of WS and PsPD arrays, suggested that is worth combining and jointly inverting data obtained with arrays that differ in depth of investigation and resolution; it delivered an imaging that is the result of the combination of the vertical resolution of WS, high lateral resolution and great penetration depth of PsPD.

Furthermore, comparison between narrow scale range extractions (Fig. 7) from ERT_6 (WS and PsPD arrays) and the overlapping XZ slice from 3D_ERT_3+4 (DD array) revealed that:

- the dipole–dipole (DD) array (Fig. 7c) showed higher lateral resolution in identifying lateral heterogeneities within alluvial deposits and in delineating the saltwater contamination.

In this portion of the aquifer the variety of experimental setups tested provided an ideal opportunity to cross-validate geophysical results with extensive ground truth provided by groundwater sampling and analysis, stratigraphic, electrical conductivity, temperature and redox potential logs undertaken within WELL_81 (Fig. 7). ERT_6 and 3D_ERT_3+4 revealed WELL_81 is localized 50 m west of a saltwater contamination (Figs. 6 and 7). This is the reason why the well intercepts brackish groundwater rather than salt groundwater. WELL_81 logs found at 11 m of depth a drop in resistivity (EC log), along with an increase of temperature and a decrease of redox potential of groundwater (Fig. 7). This well transition zone occurs in a portion of the aquifer in which, based on the bulk resistivity indicated by the ERT surveys, the aquifer should be characterized by coarser deposits. Specifically, maximum resistivity values can be found at a depth between 11 m and 12 m, which would indicate the likely presence of a clean sand layer contaminated by brackish water. This suggests that the distribution of saline water contaminations is a hydraulic conductivity-controlled process at the plume-scale within alluvial deposits, as shown in Fig. 8.

Comparison between the resistivity profiles extracted from the variety of experimental setups tested along WELL_81 axis and the EC log (converted into resistivity) showed that 2D PsPD and 2D H (Fig. 9) revealed the clean sand layer at 11 m of depth, i.e., just below the transition zone between slightly brackish and moderately brackish waters. At depths $<$10 m the EC log shows similar resistivity values due to the presence of slightly brackish water with constant salinity; conversely, the profiles extracted from the geophysical models show an increase in resistivity with depth due to a decrease in clay content with depth. At depths $>$12 m, both the EC log and the profiles extracted from the geophysical models show a decrease in resistivity with depth due to the presence of moderately brackish water and the increase in salinity with depth.

Resistivity Depth Sounding (RDS), despite of its one-dimensional feature showed a drop in resistivity at the same depth. 2D WS and 3D DD showed 2 m and 1 m underestimation of depth, respectively. Comparison between the resistivity profiles along the well axis revealed that the higher is the accuracy of the geophysical method, the larger is the measured resistivity variation range (Fig. 9).

3D_ERT_3+4 (Fig. 10) provided a good correlation with WELL_81 logs. In this portion of the aquifer, deep saline waters which reach the alluvial aquifer during upward migration, diffuse and mix with the fresh groundwater of the shallow aquifer, therefore originating different degrees of groundwater salinity within the aquifer, from saltwater to fresh water. Different resistivity range extractions from the 3D resistivity block can be related to different degrees of groundwater salinity (Fig. 10a–c). Here, the 3D geophysical imaging cross-validated by well logs provided the opportunity to map the irregular-shaped, shallow, saltwater to highly brackish water plume contaminating the alluvial aquifer. The saltwater to highly brackish water plume, which contaminates a sandy body within the alluvial deposits corresponds to the plume extracted from 3D_ERT_3+4 (4–9.3 ohm·m, Fig. 10a). This plume was detected by the 3D survey only; indeed, this survey is able to generate a more complete and accurate model with respect to 1D and 2D surveys. The 2013 3D resistivity block (3rd June 2013) provides good correlation with Well_81 logs (5th June 2013) (Fig. 10). Moderately brackish water shows lower redox potential and higher temperature than the overlying slightly brackish water.

Time-lapse monitoring of the saltwater to highly brackish water plume contaminating the alluvial aquifer was carried out by inverting the two data sets collected in late spring 2013 and 2015. It revealed the regions of the model in which change has occurred in terms of electrical

resistivity. A decrease in size of the saltwater to highly brackish water plume (Figs. 10a and 11a) and an increase in resistivity values of the alluvial aquifer (Figs. 10b,c and 11b,c) due to groundwater salinity dilution during late spring of 2015 have been observed. This is consistent with the percentage ratio between 2015 and 2013 resistivity block models (Fig. 12): the isosurface 100% (Fig. 12b) suggests the region of the model where no change has occurred between 2015 and 2013; differently, the isosurface 105% (Fig. 12c) suggests the region of the model where saltwater dilution has occurred between 2015 and 2013 (i.e., 5% higher resistivity values). In addition, the isosurface 105% (Fig. 12c) also suggests a decrease in resistivity values of the clayey and silty cover deposits during late spring of 2015 due to previous day rainfall.

7. Discussion

Although the interpretation of electromagnetic and resistivity anomalies is not always straightforward (Van Schoor, 2002), the cross-validation of geophysical results with extensive ground truth allowed definition of the general hydrogeological setting of the investigated area, as well as detailed investigation of localized and restricted zones of the aquifer which are crucial elements for the understanding of the saltwater contamination process. Geophysical surveys revealed the presence of sharp and irregular contact between the alluvial aquifer and the underlying hydrogeological bedrock. This is characterized by morphological irregularities, which are likely to have been shaped either by tectonics (Vogherese Fault zone) and/or by the paleo-river's erosion. Although, in the southern investigated area (south of the fault) the thickness of the aquifer varies between 10 and 30 m, the bedrock depth increases northward due to the Vogherese Fault. These evidences are consistent with well observations regarding bedrock depth. Geophysical results allowed achieving detailed localization and trace of the Vogherese Fault which appears to have an ENE-WSW orientation at the scale of the test site. In addition, geophysical surveys revealed that the bedrock is affected by saline water contaminations which are likely localized along structural discontinuities which represent preferential flow paths for the saline waters and facilitate the flow towards the alluvial aquifer.

Detailed 3D and time-lapse imaging revealed irregular-shaped shallow saltwater contaminations within the alluvial aquifer, as well as temporal variability of groundwater salinity. The overall, simplified hydrogeological conceptual model of the test site is shown in Fig. 13. This model represents the main features of the shallow aquifer as revealed by geophysical surveys cross-validated with well logs data.

The tested geophysical surveys proved to be effective techniques for the localization and characterization of localized and restricted saline water contaminations, which are crucial elements for the exploitation management of the aquifer, not only for drinking water supply, but also for agricultural and industrial use. Specifically, it is worth considering that although Very Low Frequency Electromagnetic (VLF-EM) surveys are more rapid than the more reliable Electrical Resistivity Tomography (ERT) surveys, not all saline water contaminations are detectable by VLF-EM. Only steeply-dipping and well coupled with the transmitter conductive bodies are able to generate electromagnetic (EM) anomalies. Considering only saline water contamination related anomalies, on a total of 21 anomalies revealed along the transect (Figs. 3 and 4):

- 62% of VLF-EM anomalies are consistent with ERT anomalies, while 10% are partially consistent;
- 67% of Resistivity Profiling (RP) anomalies are consistent with ERT anomalies, while 5% are partially consistent;
- on a total of 14 VLF-EM anomalies consistent with ERT anomalies and associated with saltwater contaminations with a width ranging between 8 m and 195 m, 50% are associated with saltwater contaminations boundaries, 50% are associated with saltwater contaminations bodies.

The study provided key performance indicators of electrode arrays in delineating this and similar hydrogeological settings. The merging and joint inversion of datasets from different arrays provided more accurate inverse models, as also suggested by Szalai et al., (2009) and Torrese (2020). This is due to the combination of the high vertical resolution of Wenner-Schlumberger (WS), high lateral resolution of dipole–dipole

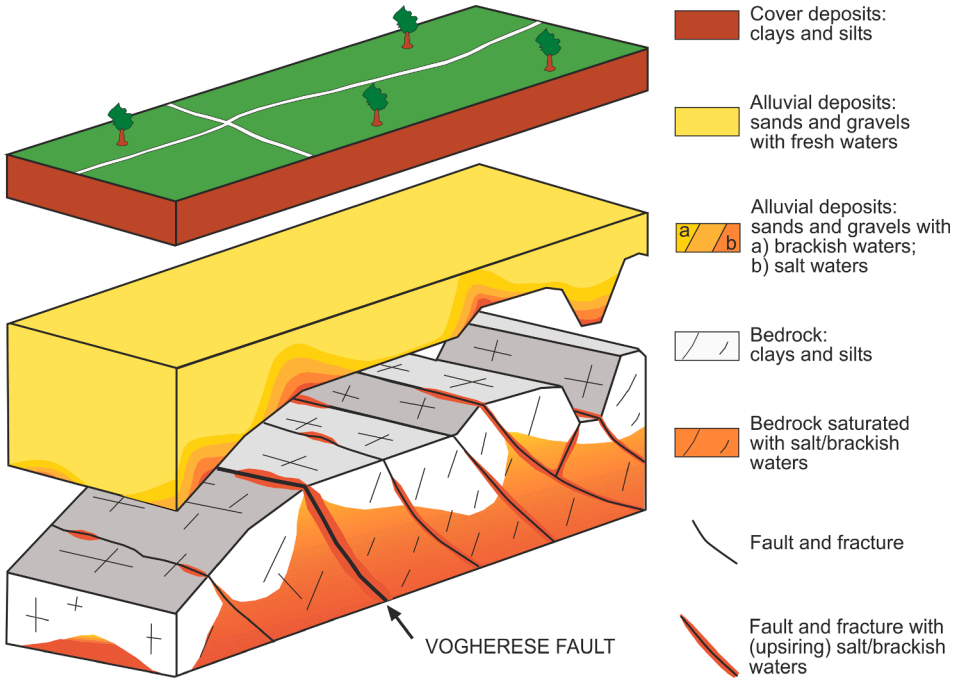

Fig. 13. Simplified hydrogeological conceptual model of the test site as revealed by geophysical surveys cross-validated with well logs data.

(DD) and Pseudo-Pole–Dipole (PsPD). In presence of flat contact between the aquifer and the underlying bedrock, the WS array achieved better detectability and imaging. Otherwise, in presence of sharp and irregular contact between the aquifer and the underlying bedrock and of localized and restricted saline water contaminations, as found in most of the investigated area, DD and PsPD arrays provided better detectability and imaging.

The study confirmed that the main drawback of Electrical Resistivity Tomography (ERT) method in such a hydrogeological context is that it is not always possible to distinguish between a morphological irregularity of the clayey bedrock and a localized and restricted saline water contamination. This is due to the fact that saline water filled coarse deposits may have an electrical resistivity very close to a clayey bedrock. Moreover, in the absence of a specific calibration (well), the resistivity range to be associated with the saline water contamination is not known. Overall, at the investigated test site, saltwater-saturated clayey bedrock shows resistivity values lower than 3 ohm·m, while saltwater-saturated sandy alluvial deposits show resistivity values ranging between 3 ohm·m and 8 ohm·m; brackish water saturated alluvial deposits show resistivity values $>$ 8 ohm·m. Even if these ranges of values can be considered representative for such a hydrogeological setting, it is worth underlining that the resistivity of such hydrogeological bodies does not depend on the water conductivity only, but also on porosity and clay content of the solid material. Moreover, the resistivity signature depends even on the size of the body in relation to its depth and on the contrast between the resistivity of the body and that of the surrounding rock. This is the reason why the same hydrogeological body can show slightly different resistivity values even in the same site.

Contamination from saline waters is not spatially and vertically homogeneous within the alluvial aquifer as also highlighted by the hydrochemical investigations. This non-homogeneity is likely to be affected by different factors like the aperture of the discontinuities within the hydrogeological bedrock, the hydraulic conductivity of the aquifer, as well as seasonal variations in terms of fresh water recharge and groundwater pumping. The hypothesis that water salinity degree and spatial distribution of saline water contaminations is a hydraulic conductivity-controlled process at the plume-scale within alluvial deposits was verified by undertaking a lithological parameterization from geophysical results. Specifically, we estimated the clay content of the alluvial deposits affected by the brackish water plume investigated by 1D to 4D electrical resistivity surveys and cross-validated with WELL_81 logs. Given the presence of groundwater at different salinity conditions, we used the algorithm proposed by Ryjov and Sudoplatov (1990). This algorithm can be used to estimate the clay content in clayey-sandy formations knowing the resistivity of the formation and the salinity of the groundwater (Shevnin et al., 2006, 2007; Rainone et al., 2015). The estimation was based on the bulk resistivity extracted from 3D_ERT_3+4 in correspondence of WELL_81 axis (orange profile in Fig. 9) and the pore water electrical conductivity obtained from WELL_81 resistivity log (purple profile in Fig. 9). An indicative estimate of clay content (cc, valid for cation exchange capacity (CEC) of clay = 1.73 g/l, clay porosity = 0.55; sand porosity = 0.22, radius of clay pores = $3{\cdot}10^{-9}$ m) was obtained along the well axis (Fig. 9). This estimate suggests a decrease in clay content with depth (as indicated also by the stratigraphic log) ranging from $>$ 13% to $<$ 5% with the exception of the presence of a clean sand layer between 11 m and 12 m of depth (Figs. 7 and 9). The presence of this layer is also suggested by the corrected formation factor (F_c) computed along the well axis by applying the Johnson et al. (1986) modification of the Waxman and Smits equation (Waxman and Smits, 1968)

$$C_t = \frac{1}{F_c}\left(C_{w+}\frac{2C_s}{\Lambda}\right) \quad (4)$$

where C_t is the bulk electrical conductivity of the formation (extracted along the well axis from 3D_ERT_3+4, orange profile in Fig. 9), F_c is the corrected formation factor, C_w is the electrical conductivity of pore water, $C_s = 1$ μS (assumed as a representative value from Wildenschild et al., 2000), is the surface electrical conductivity of the clay, $\Lambda = 8$ μm (assumed as a representative value from Wildenschild et al., 2000) is the length parameter (weighted volume to surface area ratio, that is a measure of the dynamically interconnected pore size).

Two-dimensional and three-dimensional ERT surveys agree with well logs in indicating that deep saline paleo-waters show a dilution during upward migration. This is due to the mixing with shallow fresh groundwater; furthermore, the hydrodynamic flow of shallow fresh groundwater would tend to relegate the highly mineralized groundwater to the lower sections of the aquifer.

Time-lapse ERT surveys provided some suggestions about the temporal variability of groundwater salinity. Groundwater salinity dilution revealed by the 2015 block model (Figs. 11 and 12) with respect to the 2013 block model (Figs. 10 and 12) is likely due to 52% lower rainfall during spring 2015 with respect to spring 2013. The fact that the temporal variability of groundwater salinity is connected to the variability in the discharge of uprising saltwater suggests that the uprise of saltwater is likely to be induced by an increase in hydraulic head within the main Apennine groundwater following rainfall or snow melting events. This system seems to be in hydraulic connection with a deeper aquifer that hosts saline waters. Pilla et al. (2010) and Re and Zuppi (2011) suggested a pressure transfer, through a piston flow mechanism, which can produce a mass transfer where saline waters are forced to rise along discontinuities and reach the shallow aquifer. That was observed to coincide with aquifer recharge (maximum values of water table). On the other hand, the 2015 block model shows a decrease in resistivity of the upper clayey deposits (Fig. 12). This is due to previous day rainfall, affecting only very shallow resistivity values. Forthcoming studies based on continuous piezometric and hydrochemical monitoring of the alluvial aquifer groundwater correlated to rainfall or snow melting events in the nearby Apennines will allow to verify the piston flow mechanism based hypothesis.

Furthermore, next research steps to enhance the present study will concern the extension of the geophysical study in other areas of the Oltrepò Pavese plain sector. Further transects crossing the fault zone and detailed investigations will be carried out at selected test sites. This will allow us to verify the extent of the hydrogeological conditions revealed by this study. The geophysical study will be integrated with an in-depth hydrochemical study, accompanied by continuous piezometric and hydrochemical monitoring of the alluvial aquifer groundwater. This will be aimed at obtaining further insights into the spatial distribution of saline water contaminations and the mechanisms underlying the upward migration of saline paleo-water, its diffusion and mixing with the fresh groundwater of the shallow aquifer.

8. Conclusions

We presented new results of the application of 1D-4D electrical resistivity and electromagnetic surveys for the delineation of aquifer geometry and the detection of saline paleo-water uprising along structural discontinuities. These geophysical surveys were undertaken at the alluvial aquifer of the Oltrepò Pavese plain sector (Po Valley, Northern Italy). At the investigated test site, the alluvial aquifer is strongly conditioned by the presence of an important tectonic discontinuity whose localization and trace were better defined by this study. This fault is responsible for the sudden deepening that affects the hydrogeological bedrock and is also responsible for the uprising of deep, saline paleo-waters which strongly influences the chemistry of groundwater.

During the campaign a variety of experimental setups were tested. This provided an ideal opportunity to cross-validate geophysical results with extensive ground truth provided by groundwater sampling and analysis, stratigraphic, electrical conductivity, temperature and redox potential logs undertaken within the wells. It also permitted an

assessment of the usability of electrical and electromagnetic surveys in such a complex hydrogeological setting.

Geophysical surveys revealed the presence of sharp and irregular contact between the alluvial aquifer and the underlying hydrogeological bedrock. This is characterized by morphological irregularities, which are likely to have been shaped either by tectonics and/or by the paleo-river's erosion. The bedrock is affected by saline water contaminations which are likely localized along structural discontinuities which represent preferential flow paths for the saline waters and facilitate the flow towards the alluvial aquifer. Detailed 3D and time-lapse imaging revealed irregular-shaped shallow saltwater contaminations within the alluvial aquifer, as well as temporal variability of groundwater salinity. Contamination from saline waters is not spatially and vertically homogeneous within the alluvial aquifer. Spatial distribution of contaminations and salinity degree are likely to be affected by different factors like the aperture of the discontinuities within the hydrogeological bedrock, the hydraulic conductivity of the aquifer, as well as seasonal variations in terms of fresh water recharge. The temporal variability of groundwater salinity revealed by time-lapse imaging would suggest that the uprise of deep, saline paleo saltwater is likely to be induced by a pressure transfer mechanism that may force saline waters to rise along discontinuities and reach the shallow alluvial aquifer.

The results from our study are applicable in similar hydrogeological contexts where the aquifer's contamination by saltwater is caused by mixing of freshwaters with brines or where the fossil salt waters, located different kilometers far from the coastline, are remainder of ancient marine ingressions.

CRediT authorship contribution statement

Patrizio Torrese: Conceptualization, Methodology, Validation, Formal analysis, Investigation, Resources, Writing - original draft, Writing - review & editing, Supervision, Project administration. **Giorgio Pilla:** Conceptualization, Validation, Investigation, Resources, Writing - original draft, Project administration, Funding acquisition.

Declaration of Competing Interest

The authors declare that they have no known competing financial interests or personal relationships that could have appeared to influence the work reported in this paper.

Acknowledgements

The study was developed in the framework of the convention between Dipartimento di Scienze della Terra e dell'Ambiente of Università di Pavia (P.I. Giorgio Pilla) and Provincia di Pavia - Settore Tutela Ambientale with the collaboration of Comune di Casteggio, Comune di Santa Giuletta, Comune di Montebello della Battaglia, the company Pavia Acque Srl and the company Casteggio Lieviti Srl.

The authors are grateful to Marica Bersan, Massimiliano Bordoni, Luca Bovolenta, Alessandro Sartirana and Francesco Tosi for their support in data collection, processing and editing. We would like to thank the people that allowed us to access and sample the investigated area.

The authors wish to thank the Editor-in-Chief Corrado Corradini, the Associate Editor Steve Worthington and three anonymous referees who kindly reviewed the earlier version of this manuscript and provided valuable suggestions and comments, greatly improving the quality of the manuscript.

References

AGIP, 1994. Acque dolci sotterranee. AGIP S.p.A.. Direzione Generale Servizi Centrali per l'Esplorazione, 515.

Adepelumi, A.A., Yi, M.-J., Kim, J.-H., Ako, B.D., Son, J.S., 2006. Integration of surface geophysical methods for fracture detection in crystalline bedrocks of southwestern Nigeria. Hydrogeol. J. 14 (7), 1284–1306. https://doi.org/10.1007/s10040-006-0051-2.

Akouvi, A., Dray, M., Violette, S., de Marsily, G., Zuppi, G.M., 2008. The sedimentary coastal basin of Togo: example of a multilayered aquifer still influenced by a palaeo–seawater intrusion. Hydrogeol. J. 16 (3), 419–436.

Al-Tarazi, E., Abu Rajab, J., Al-Naqa, A., El-Waheidi, M., 2008. Detecting leachate plumes and groundwater pollution at Ruseifa municipal landfill utilizing VLF-EM method. J. Appl. Geophys. 65 (3-4), 121–131.

Arato, A., Godio, A., Sambuelli, L., 2014. Staggered grid inversion of cross hole 2-D resistivity tomography. J. Appl. Geophys. 107, 60–70.

Athanasiou, E.N., Tsourlos, P.I., Papazachos, C.B., Tsokas, G.N., 2007. Combined weighted inversion of electrical resistivity data arising from different array types. J. Appl. Geophys. 62 (2), 124–140.

Beard, L.P., Lutro, O., 2000. Airborne geophysics and infrastructure planning – A Case Study. J. Environ. Eng. Geophys. 5 (2), 1–10.

Bersan, M., Pilla, G., Dolza, G., Torrese, P., Ciancetti, G., 2010. The uprising of deep saline waters into the Oltrepò Pavese (Northern Italy) aquifer: early results. Ital. J. Eng. Geol. Environ. 1, 7–22.

Boni, A., 1967. Note illustrative della Carta Geologica d'Italia. F. 59 Pavia. 68 pp., Roma.

Bonnesen, E.P., Larsen, F., Sonnenborg, T.O., Klitten, K., Stemmerik, L., 2009. Deep saltwater in Chalk of North-West Europe: Origin, interface characteristics and development over geological time. Hydrogeology Journal, 17, 1643-1663. 10.1007/s10040-009-0456-9.

Bouchaou, L., Michelot, J.L., Qurtobi, M., Zine, N., Gaye, C.B., Aggarwal, P.K., Marah, H., Zerouali, A., Taleb, H., Vengosh, A., 2009. Origin and residence time of groundwater in the Tadla Basin (Morocco) using multiple isotopic and geochemical tools. J. Hydrol. 379 (3-4), 323–338. https://doi.org/10.1016/j.jhydrol.2009.10.019.

Bowling, J.C., Rodriguez, A.B., Harry, D.L., Zheng, C., 2005. Delineating alluvial aquifer heterogeneity using resistivity and GPR Data. Groundwater 43 (6), 890–903. https://doi.org/10.1111/j.1745-6584.2005.00103.x.

Braga, G., Cerro, A., 1988. Le strutture sepolte della pianura pavese e le relative influenze sulle risorse idriche sotterranee. Atti Tic. Sc. Terra 31, 421–433.

Buvat, S., Schamper, C., Tabbagh, A., 2013. Approximate three-dimensional resistivity modelling using Fourier analysis of layer resistivity in shallow soil studies. Geophys. J. Int. 194 (1), 158–169.

Cameron, E., Pilla, G., Stella, F.A., 2018. Application of statistical classification methods for predicting the acceptability of well-water quality. Hydrogeol. J. 26, 1099–1115.

Cassiani, G., Godio, A., Stocco, S., Villa, A., Deiana, R., Frattini, P., Rossi, M., 2009. Monitoring the hydrologic behaviour of a mountain slope via time-lapse electrical resistivity tomography. Near Surf. Geophys. 7 (5-6), 475–486.

Cavanna, F., Marchetti, G., Vercesi, P.L., 1998. Idrogeomorfologia e insediamenti a rischio ambientale. Il caso della pianura dell'Oltrepò Pavese e del relativo margine collinare. Fondazione Lombardia Ambiente, 14 72, Isabel Litografia, Gessate (MI).

Conti, A., Sacchi, E., Chiarle, M., Martinelli, G., Zuppi, G.M., 2000. Geochemistry of the formation water of the Po plain (northern Italy): an overview. Appl. Geochem. 15, 51–65.

Coscia, I., Greenhalgh, S.A., Linde, N., Doetsch, J., Marescot, L., Günther, T., Vogt, T., Green, A.G., 2011. 3D crosshole ERT for aquifer characterization and monitoring of infiltrating river water. Geophysics 76 (2), G49–G59. https://doi.org/10.1190/1.3553003.

Dahlin, T., Loke, M.H., 1998. Resolution of 2-D Wenner resistivity imaging as assessed by numerical modelling. J. Appl. Geophys. 38 (4), 237–249.

Daily, W., Owen, E., 1991. Crosshole resistivity tomography. Geophysics 56, 1228–1235.

Daily, W., Ramirez, A., LaBrecque, D., Nitao, J., 1992. Electrical resistivity tomography of vadose water movement. Water Resour. Res. 28 (5), 1429–1442.

Darling, W.G., Edmunds, W.M., Smedley, P.L., 1997. Isotopic evidence for palaeowaters in the British Isles. Applied Geochemistry, 12, 6, 813-829, ISSN 0883-2927, https://doi.org/10.1016/S0883-2927(97)00038-3.

De la Vega, M., Osella, A., Lascano, E., 2003. Joint inversion of Wenner and dipole-dipole data to study a gasoline-contaminated soil. J. Appl. Geophys. 54 (1-2), 97–109.

Desiderio, G., Rusi, S., 2004. Idrogeologia e idrogeochimica delle acque mineralizzate dell'Avanfossa Abruzzese Molisana. Boll. Soc. Geol. It. 123, 373–389.

Dever, L., Travi, Y., Barbecot, F., Marlin, C., Gibert, E., 2001. Evidence for palaeowaters in the coastal aquifers of France. Geol. Soc. London, Spec. Publ. 189 (1), 93–106. https://doi.org/10.1144/GSL.SP.2001.189.01.07.

Fraser, D.C., 1969. Contouring of VLF-EM data. Geophysics 34 (6), 958–967.

Fraser, D.C., 1981. A review of some useful algorithms in geophysics. Can. Inst. Min. Trans. 74 (828), 76–83.

Gómez, E., Larsson, M., Dahlin, T., Barmen, G., Rosberg, J.-E., 2019. Alluvial aquifer thickness and bedrock structure delineation by electromagnetic methods in the highlands of Bolivia. Environ. Earth Sci. 78 (3) https://doi.org/10.1007/s12665-019-8074-x.

Gnaneshwar, P., Shivaji, A., Srinivas, Y., Jettaiah, P., Sundararajan, N., 2011. Very-low-frequency electromagnetic (VLF-EM) measurements in the Schirmacheroasen area, East Antarctica. Polar Sci. 5 (1), 11–19. https://doi.org/10.1016/j.polar.2010.09.001.

Griffiths, D.H., Barker, R.D., 1993. Two-dimensional resistivity imaging and modeling in areas of complex geology. J. Appl. Geophys. 29, 211–226.

Guérin, R., Benderitter, Y., 1995. Shallow karst network exploration using MT-VLF and DC resistivity methods. Geophys. Prospect. 43 (5), 635–653.

Guérin, R., Bégassat, P., Benderitter, Y., David, J., Tabbagh, A., Thiry, M., 2004. Geophysical study of the industrial waste land in Mortagne-du-Nord (France) using electrical resistivity. Near Surf. Geophys. 2 (3), 137–143.

Hinsby, K., Harrar, W.G., Nyegaard, P., Konradi, P.B., Rasmussen, E.S., Bidstrup, T., Gregersen, U., Boaretto, R., 2001, The Ribe Formation in western Denmark — Holocene and Pleistocene groundwaters in a coastal Miocene sand aquifer. In book:

Palaeowaters in Coastal Europe: evolution of groundwater since the late Pleistocen, Publisher: The Geological Society, Editors: C M Edmunds, C J Milne.
Jamal, N., Singh, N.P., 2018. Identification of fracture zones for groundwater exploration using very low frequency electromagnetic (VLF-EM) and electrical resistivity (ER) methods in hard rock area of Sangod Block, Kota District, Rajasthan, India. Groundwater for Sustainable Development, 7, 195-203, ISSN 2352-801X, https://doi.org/10.1016/j.gsd.2018.05.003.
Johnson, D.L., Koplik, J., Schwartz, L.M., 1986. New pore size parameter characterizing transport in porous media. Phys. Rev. Lett. 57 (20), 2564–2567.
Kazakis, N., Pavlou, A., Vargemezis, G., Voudouris, K.S., Soulios, G., Pliakas, F., Tsokas, G., 2016a. Seawater intrusion mapping using electrical resistivity tomography and hydrochemical data. An application in the coastal area of eastern Thermaikos Gulf, Greece. Sci. Total Environ. 543, 373–387. https://doi.org/10.1016/J.SCITOTENV.2015.11.041.
Kazakis, N., Vargemezis, G., Voudouris, K.S., 2016. Estimation of hydraulic parameters in a complex porous aquifer system using geoelectrical methods. Science of The Total Environment, 550, 742-750, ISSN 0048-9697, https://doi.org/10.1016/j.scitotenv.2016.01.133.
Kneisel, C., 2006. Assessment of subsurface lithology in mountain environments using 2D resistivity imaging. Geomorphology 80 (1–2), 32–44. https://doi.org/10.1016/j.geomorph.2005.09.012.
Kuras, O., Pritchard, J.D., Meldrum, P.I., Chambers, J.E., Wilkinson, P.B., Ogilvy, R.D., Wealthall, G.P., 2009. Monitoring hydraulic processes with Automated time-Lapse Electrical Resistivity Tomography (ALERT). Comptes Rendus Geosci. - Special Issue on Hydrogeophys. 341 (10-11), 868–885.
LaBrecque, D.J., Miletto, M., Daily, W., Ramirez, A., Owen, E., 1996. The effects of noise on Occam's Inversion of resistivity tomography data. Geophysics 61 (2), 538–548.
Loke, M.H., Acworth, I., Dahlin, T., 2003. A comparison of smooth and blocky inversion methods in 2-D electrical imaging surveys. Explor. Geophys. 34 (3), 182–187.
Loke, M.H., Barker, R.D., 1996. Rapid least-squares inversion of apparent resistivity pseudosections by a quasi-Newton method. Geophys. Prospect. 44 (1), 131–152. https://doi.org/10.1111/j.1365-2478.1996.tb00142.x.
Marandi, A., Vallner, L., 2010. Upconing of saline water from the crystalline basement into the Cambrian-Vendian aquifer system on the Kopli Peninsula, northern Estonia. Estonian J. Earth Sci. 59, 277–287. https://doi.org/10.3176/earth.2010.4.04.
Meyerhoff, S.B., Karaoulis, M., Fiebig, F., Maxwell, R.M., Revil, A., Martin, J.B., Graham, W.D., 2012. Visualization of conduit-matrix conductivity differences in a karst aquifer using time-lapse electrical resistivity. Geophys. Res. Lett. 39, L24401. https://doi.org/10.1029/2012GL053933.
Meyerhoff, S.B., Maxwell, R.M., Revil, A., Martin, J.B., Karaoulis, M., Graham, W.D., 2014. Characterization of groundwater and surface water mixing in a semiconfined karst aquifer using time-lapse electrical resistivity tomography. Water Resour. Res. 50 (3), 2566–2585. https://doi.org/10.1002/2013WR013991.
Morelli, G., LaBrecque, D.J., 1996. Advances in ERT inverse modelling. Eur. J. Environ. Eng. Geophys. Soc. 1 (2), 171–186.
Ohwoghere-Asuma, O., Chinyem, I.F., Aweto, K.E., Iserhien-Emekeme, R., 2020. The use of very low-frequency electromagnetic survey in the mapping of groundwater condition in oporoza-gbamaratu area of the Niger Delta. Appl Water Sci 10, 164 (2020). https://doi.org/10.1007/s13201-020-01244-w.
Ogilvy, R.D., Lee, A.C., 1991. Interpretation of VLF-EM inphase data using current density pseudosections. Geophys. Prospect. 39, 567–580.
Paál, G., 1965. Ore prospecting based on VLF radio signals. Geoexploration 3 (3), 139–147.
Parker, M.E., 1980. VLF electromagnetic mapping for strata-bound mineralization near Aberfeldy, Scondland. Trans. Inst. Min. Metall. Sect. B 89, B123–B133.
Paterson, N.R., Ronka, V., 1971. Five years of surveying with the very low frequency electromagnetic method. Geoexploration 9, 7–26.
Pellegrini, L., Vercesi, P.L., 1995. Considerazioni morfotettoniche sulla zona a sud del Po tra Voghera (PV) e Sarmato (PC). Atti Tic. Sc. Terra, 38.
Phillips, W.J., Richards, W.E., 1975. A study of the effectiveness of the VLF method for the location of narrow mineralized zones. Geoexploration 13, 215–226.
Pilla, G., Torrese, P., Bersan, M., 2010. Application of hydrochemical and preliminary geophysical surveys within the study of the saltwater uprising occurring in the Oltrepò Pavese plain aquifer. Bollettino di Geofisica Teorica e Applicata 51 (4), 301–323.
Pilla, G., Sacchi, E., Ciancetti, G., 2007. Hydrogeologic, hydrochemical and isotopic groundwater investigation in the plain of the Oltrepò Pavese region (Southern Lombardy, Italy). Giornale di Geologia Applicata 5, 59–74.
Razafindratsima, S., Lataste, J.-F., 2014. Estimation of the error made in Pole-Dipole Electrical Resistivity Tomography depending on the location of the remote electrode: Modeling and field study. J. Appl. Geophys. 100, 44–57.
Schrott, L., & Sass, O., 2008. Application of field geophysics in geomorphology: Advances and limitations exemplified by case studies. Geomorphology, 93(1–2), 55–73. https://doi.org/10.1016/j.geomorph HYPERLINK "https://doi.org/10.1016/j.geomorph.2006.12.024".2006.12.024.
Spiegel, R.J., Sturdivant, V.R., Owen, T.E., 1980. Modeling resistivity anomalies from localized voids under irregular terrain. Geophysics 45 (7), 1164–1183.
Nanni, T., Zuppi, G.M., 1986. Acque salate e circolazione profonda in relazione all'assetto strutturale del fronte adriatico e padano dell'Appennino. Mem. Soc. Geol. It. 35, 979–986.
Rainone, M.L., Rusi, S., Torrese, P., 2015. Mud Volcanoes in Central Italy: Subsoil Characterization through a Multidisciplinary Approach. Geomorphology 234, 228–242. https://doi.org/10.1016/j.geomorph.2015.01.026.
Ramesh Babu, V., Ram, S., Sundararajan, N., 2007. Modeling of magnetic and VLF-EM with an application to basement fracturesda case study from Raigad, India. Geophysics 71, 133e140.
Re, V., Zuppi, G.M., 2011. Influence of precipitation and deep saline groundwater on the hydrological systems of Mediterranean coastal plains: a general overview. Hydrol. Sci. J. 56 (6), 966–980.
Regione Lombardia and ENI Divisione AGIP, 2002. Geologia degli acquiferi padani della Regione Lombardia. A cura di Carcano C, Piccin A (eds), S.E.L.C.A. Firenze.
Ryjov, A.A., Sudoplatov, A.D., 1990. The calculation of specific electrical conductivity for sandy – clayed rocks and the usage of functional cross–plots for the decision of hydrogeological problems. In: In the book: "Scientific and technical achievements and advanced experience in the field of geology and mineral deposits research". Moscow, pp. 27–41.
Ritz, M., Robain, H., Pervago, E., Albouy, Y., Camerlynck, C., Descloitres, M., Mariko, A., 1999. Improvement to resistivity pseudosection modelling by removal of near-surface heterogeneity effects: application to a soil system in South Cameroon. Geophys. Prospect. 47, 85–101.
Robain, H., Albouy, Y., Dabas, M., Descloitres, M., Camerlynck, C., Mechler, P., Tabbagh, A., 1999. The location of infinite electrodes in pole–pole electrical surveys: consequences for 2D imaging. J. Appl. Geophys. 41 (4), 313–333.
Saydam, A.S., 1981. Very low frequency electromagnetic interpretation using tilt angle and ellipticity measurements. Geophysics 46 (11), 1594–1605.
Seaton, W. J. and Burbey, T. J., 2002. Evaluation of two-dimensional resistivity methods in a fractured crystalline-rock terrane. Journal of Applied Geophysics, 51(1): PII S0926-9851(02)00212-4. DOI: 10.1016/S0926-9851(02)00212-4.
Shevnin, V., Delgado-Rodríguez, O., Mousatov, A., Ryjov, A., 2006. Estimation of hydraulic conductivity on clay content in soil determined from resistivity data. Geofísica Internacional 45 (3), 195–207.
Shevnin, V., Mousatov, A., Ryjov, A., Delgado-Rodriquez, O., 2007. Estimation of clay content in soil based on resistivity modeling and laboratory measurements. Geophys. Prospect. 55, 265–275. https://doi.org/10.1111/j.1365-2478.2007.00599.x.
Smith, D.L., 1986. Application of the pole–dipole resistivity technique to the detection of solution cavities beneath highways. Geophysics 51 (3), 833–837.
Sundararajan, N., Ramesh Babu, V., Shiva Prasad, N., Srinivas, Y., 2006. VLFPROSda Matlab code for processing of VLF-EM data. Comput. Geosci. 32, 1806e1813.
Szalai, S., Szarka, L., 2008. Parameter sensitivity maps of surface geoelectric arrays I. Linear arrays. Acta Geodaetica et Geophysica Hungarica 43 (4), 419–437. https://doi.org/10.1556/AGeod.43.2008.4.4.
Szalai, S., Novak, A., Szarka, L., 2009. Depth of Investigation and Vertical Resolution of Surface Geoelectric Arrays. J. Environ. Eng. Geophys. 14 (1), 15–23. https://doi.org/10.2113/JEEG14.1.15.
Stueber, A.M., Saller, A., Ishida, H., 1998. Origin, Migration, and Mixing of Brines in the Permian Basin: Geo chemical Evidence from the Eastern Central Basin Platform, Texas. AAPG Bull. 82, 1652–1672.
Torrese, P., 2020. Investigating karst aquifers: Using pseudo 3-D electrical resistivity tomography to identify major karst features. J. Hydrol. 580, 124257. https://doi.org/10.1016/j.jhydrol.2019.124257.
Torrese, P., Pozzobon, R., Rossi, A.P., Unnithan, V., Sauro, F., Borrmann, D., Lauterbach, H., Santagata, T., 2021. Detection, imaging and analysis of lava tubes for planetary analogue studies using electric methods (ERT). Icarus 357, 114244. https://doi.org/10.1016/j.icarus.2020.114244.
Van Schoor, M., 2002. Detection of sinkholes using 2D electrical resistivity imaging. J. Appl. Geophys. 50 (4), 393–399. https://doi.org/10.1016/S0926-9851(02)00166-0.
Vogelgesang, J.A., Holt, N., Schilling, K.E., Gannon, M., Tassier-Surine, S., 2020. Using high-resolution electrical resistivity to estimate hydraulic conductivity and improve characterization of alluvial aquifers. J. Hydrol. 580, 0022–1694. https://doi.org/10.1016/j.jhydrol.2019.123992.
Waxman, M.H., Smits, L.J.M., 1968. Electrical Conductivities in Oil-Bearing Shaly Sands. SPE J. 8, 107–122. https://doi.org/10.2118/1863-A.
Wildenschild, D., Roberts, J.J., Carlberg, E.D., 2000. On the relationship between microstructure and electrical and hydraulic properties of sand-clay mixtures. Geophys. Res. Lett. 27 (19), 3085–3088.